



HAL
open science

Formation of murtoos by repeated flooding of ribbed bedforms along subglacial meltwater corridors

Jean Vérité, E. Ravier, Olivier Bourgeois, Paul Bessin, Stephen J Livingstone, Christopher D Clark, Stéphane Pochat, Régis Mourgues

► To cite this version:

Jean Vérité, E. Ravier, Olivier Bourgeois, Paul Bessin, Stephen J Livingstone, et al.. Formation of murtoos by repeated flooding of ribbed bedforms along subglacial meltwater corridors. *Geomorphology*, 2022, 408, pp.108248. 10.1016/j.geomorph.2022.108248 . hal-04331955

HAL Id: hal-04331955

<https://hal.science/hal-04331955>

Submitted on 12 Dec 2023

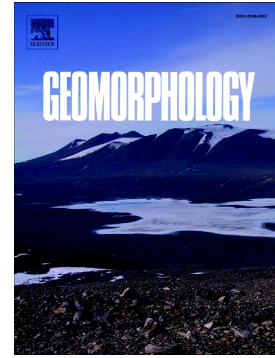
HAL is a multi-disciplinary open access archive for the deposit and dissemination of scientific research documents, whether they are published or not. The documents may come from teaching and research institutions in France or abroad, or from public or private research centers.

L'archive ouverte pluridisciplinaire **HAL**, est destinée au dépôt et à la diffusion de documents scientifiques de niveau recherche, publiés ou non, émanant des établissements d'enseignement et de recherche français ou étrangers, des laboratoires publics ou privés.

Journal Pre-proof

Formation of murtoos by repeated flooding of ribbed bedforms along subglacial meltwater corridors

Jean Vérité, Édouard Ravier, Olivier Bourgeois, Paul Bessin, Stephen J. Livingstone, Christopher D. Clark, Stéphane Pochat, Régis Mourgues



PII: S0169-555X(22)00141-6

DOI: <https://doi.org/10.1016/j.geomorph.2022.108248>

Reference: GEOMOR 108248

To appear in: *Geomorphology*

Received date: 30 November 2021

Revised date: 5 April 2022

Accepted date: 5 April 2022

Please cite this article as: J. Vérité, É. Ravier, O. Bourgeois, et al., Formation of murtoos by repeated flooding of ribbed bedforms along subglacial meltwater corridors, *Geomorphology* (2021), <https://doi.org/10.1016/j.geomorph.2022.108248>

This is a PDF file of an article that has undergone enhancements after acceptance, such as the addition of a cover page and metadata, and formatting for readability, but it is not yet the definitive version of record. This version will undergo additional copyediting, typesetting and review before it is published in its final form, but we are providing this version to give early visibility of the article. Please note that, during the production process, errors may be discovered which could affect the content, and all legal disclaimers that apply to the journal pertain.

Formation of murtoos by repeated flooding of ribbed bedforms along subglacial meltwater corridors

Jean Vérité¹, Édouard Ravier¹, Olivier Bourgeois², Paul Bessin¹, Stephen J. Livingstone³, Christopher D. Clark³, Stéphane Pochat², Régis Mourgues¹

¹ Laboratoire de Planétologie et Géosciences, UMR 6112, CNRS, Le Mans Université, Avenue Olivier Messiaen, 72085 Le Mans CEDEX 9, France

² Laboratoire de Planétologie et Géosciences, UMR 6112, CNRS, Nantes Université, 2 rue de la Houssinière, BP 92208, 44322 Nantes CEDEX 3, France

³ Department of Geography, University of Sheffield, Sheffield, UK

Corresponding author: Jean Vérité (jean.verite@univ-lemans.fr)

Keywords

Glacial geomorphology; analog modeling; subglacial hydrology, subglacial bedforms; Scandinavia

Abstract

Fluctuations in meltwater discharge below modern glaciers and ice sheets due to diurnal, seasonal and long-term temperature variations are modulated by complex interactions between subglacial drainage, basal processes and bedform development. The bed of palaeo ice sheets contains a variety of bedforms recording these modulations and provides an open window into the subglacial environment. Through the morphometric analysis of natural and experimental bedforms, respectively mapped along Scandinavian meltwater corridors and produced in a physical model simulating transitory subglacial water flow, we observe a morphological and genetic bedform continuum corresponding to the progressive transformation of ribbed bedforms into murtoos. Two alternating drainage configurations, related to repeated subglacial flooding events, are involved in this transformation: (i) significant meltwater discharge, high hydraulic connectivity and ice-bed decoupling during flooding events lead to hydraulic alteration of ribbed bedforms by erosion, sediment deposition and channel incision, while (ii) limited meltwater flow, low hydraulic connectivity and ice-bed recoupling that follow flooding events lead to their deformational reshaping into murtoos. The degree of transformation of ribbed bedforms into murtoos can be quantified by combining two dimensionless morphometric parameters (circularity and sinuosity) and provides a convenient proxy to constrain magnitudes, durations and/or frequencies of subglacial floods in palaeo-meltwater corridors.

1 Introduction

The reconstruction of subglacial hydrological systems and routes is critical for inferring basal thermal regimes (Kleman and Hattestrand, 1999; Irvine-Fynn et al., 2011; Smith-Johnsen et al., 2020), meltwater discharge fluctuations (Moon et al., 2014; Simkins et al., 2017; O'Connor et al., 2020), flow dynamics (Iken and Bindenschadler, 1986; Anandakrishnan and Alley, 1997; Bell et al., 2007; Schroeder et al., 2013; Williams et al., 2020) and frontal ablation (Slater et al., 2015; Fried et al., 2019) of ice masses. Palaeoglaciology can help reconstruct past subglacial hydrological systems from the geomorphological imprints left behind by palaeo-ice sheets to understand their evolution and dynamics during deglaciation (St-Onge, 1984; Cofaigh, 1996; Rampton et al., 2000; Utting et al., 2009; Storrar and Livingstone, 2017; Lewington et al., 2019; Ojala et al., 2019; Coughlin et al., 2020) and extrapolate these findings to contemporary ice sheets. New high-resolution (<5 m) Digital Elevation Models (DEMs) based on aerial LiDAR data enable the glacial geomorphological records to be more accurately deciphered through revised mapping, identification of previously unrecognized landforms and more accurate morphometric analyses.

Recent studies conducted in Scandinavia unraveled hitherto unidentified subglacial bedforms characterized by a triangular shape. These bedforms, referred to as murtoos (Ojala et al., 2019; Peterson Becher and Johnson, 2021) or triangle-type murtoos (Ojala et al., 2021), were initially called 'V-shaped hummocks' (Peterson et al., 2017) and 'triangular-shaped landforms' (Mäkinen et al., 2017). In plan view, murtoos are triangles with a longitudinal axis of symmetry parallel to the ice flow direction and a tip pointing downstream. Murtoos are 30 to 200 m long and wide, less than 5 m high and have asymmetric longitudinal profiles with sharp and steep downstream edges (Ojala et al., 2019). They are composed of subglacial traction till interbedded with lenses of sorted sandy sediments, both showing deformation related to shearing and liquefaction processes (Peterson Becher and Johnson, 2021; Ojala et al., 2021). Within single subglacial bedform fields, murtoos are commonly associated with bedforms that partially share some of their characteristics, such as a lobate or irregular/asymmetric triangular shape and asymmetric longitudinal profiles: these have been referred to as murtoo-related landforms by Ojala et al. (2021).

Previous geomorphological mapping on the bed of the former Scandinavian Ice Sheet (SIS) demonstrated that murtoos are frequently gathered in fields or corridors parallel to the former ice flow directions. Murtoo fields commonly occur in close association with eskers along hummock tracts, which are characterized by a rough texture contrasting with the surrounding streamlined glacial bed (Peterson et al., 2017; Ahokangas et al., 2021). Hummock tracts are a few kilometers wide and several to tens of kilometers long and are interpreted as routes that drained pulses of meltwater flow beneath decaying ice sheets (Peterson and Johnson, 2018). These routes were first observed as 'glaciofluvial corridors' in Canada (St-Onge, 1984; Utting et al., 2009), and were more recently referred to as 'meltwater corridors' (Lewington et al., 2019, 2020; Ojala et al., 2019; Sharpe et al., 2021), a term that we use in the article.

Murtoos have been interpreted to form by a combination of erosion, deposition and deformation of water-saturated sediments and subglacial till when large volumes of meltwater are delivered to warm subglacial beds (*Mäkinen et al., 2017; Ojala et al., 2019; Peterson Becher and Johnson, 2021; Ahokangas et al., 2021*). These periodic meltwater inputs are likely to cause flooding events overwhelming channelized or hydraulically connected distributed drainage systems along meltwater corridors (e.g., *Lewington et al., 2020; Mejía et al., 2021; Nanni et al., 2021*). Murtoo fields, forming parts of longer and wider meltwater routes, have been interpreted to represent small-scale transitional drainage systems between alternating channelized and distributed regimes, controlled by variations in the amount of meltwater (*Mäkinen et al., 2017; Ojala et al., 2019, 2021; Peterson Becher and Johnson, 2021*).

In Scandinavia, some murtoo fields are spatially associated with ribbed bedforms (**Fig. 1**), which have been referred to as ‘ribbed moraines’ (*Hughes, 1964; Lundqvist, 1969, 1989; Hättestrand and Kleman, 1999; Möller and Dowling, 2015*), with crosscutting relationships suggesting murtoos postdate the formation of the ribbed bedforms (*Ojala et al., 2019; Ahokangas et al., 2021*). The terms ‘Rogen moraine,’ ‘Asnen moraine,’ and ‘Niemisal moraine’ refer to special forms of ribbed moraines in the Lake Rogen area (*Lundqvist, 1969, 1989*), southern Småland, Sweden (*Möller and Dowling, 2015*), and in northeastern Sweden (*Lindén et al., 2008*). Ribbed bedforms are subglacially-produced ridges transverse to the ice flow direction (*Dunlop and Clark, 2006*). They are primarily thought to result from subglacial shear and bed deformation, but the context and primary driving mechanism varies between localized areas of ice-bed recoupling associated with spatial variations in water drainage and ice flow velocity under warm-based ice (*Shaw, 1979; Boulton, 1987; Lindén et al., 2008; Fowler & Chapwanya, 2014; Vérité et al., 2021*); or at the transition between cold-based and warm-based ice (*Hättestrand & Kleman, 1999*). Except for the hypothesis of *Shaw (2002)*, who invokes large-scale subglacial meltwater floods, the formation of ribbed bedforms has most commonly been related to low meltwater flow. Although spatial associations between ribbed bedforms and murtoos have been observed, a possible genetic relationship between them has not been reported yet.

Over the last decade, the emergence of numerical (*Fowler and Chapwanya, 2014; Fannon et al., 2017*) and experimental (*Lelandais et al., 2016, 2018; Vérité et al., 2021*) models have enabled the exploration of relationships between genesis and evolution of subglacial bedforms and drainage features, and ice flow dynamics and meltwater flow at the ice-bed interface. The experimental model initiated by *Lelandais et al. (2016, 2018)* and further developed by *Vérité et al. (2021)* notably contributed to better understand the link between the development of meltwater channels and ribbed bedforms and the dynamics of ice lobes and ice streams. However, neither numerical nor experimental models have simulated the formation of murtoos.

In this study, we explore the relationship between the dynamics of subglacial hydrological systems and the formation of murtoos when they are associated with ribbed bedforms. For that purpose, we mapped bedforms using selected portions of LiDAR DEMs along Scandinavian meltwater corridors. Based on the definition of new

dimensionless morphometric criteria, we compared these natural bedforms with experimental bedforms produced in an analog model, identical to that used by *Vérité et al. (2021)*. From this comparison, we derive a model for the formation of murtoos and discuss the implications for the reconstruction of meltwater corridors.

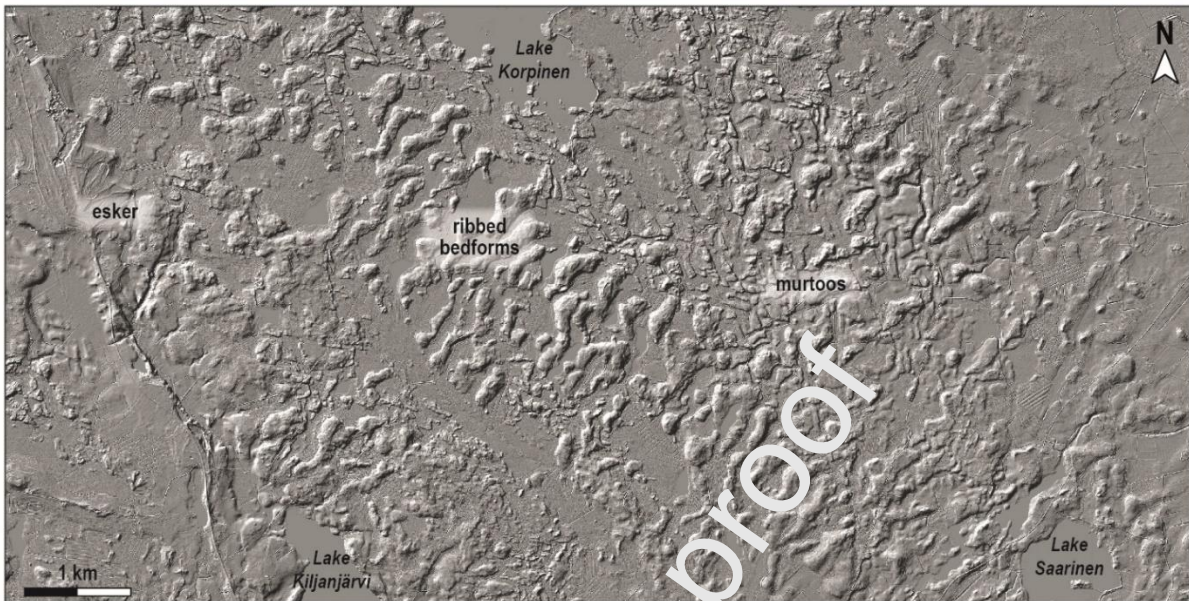


Figure 1. A spatial association between murtoos and ribbed bedforms. The field is located north of Lake Kiljanjärvi, W Finland (63°39'12"N – 24°56'41"E). Ice flow was directed towards the southeast. Ribbed bedforms (undulating ridges striking SW-NE) dominate the landscape but are interrupted in places (notably downstream from Lake Korpinen) by murtoos (downstream pointing triangular hills).

2 Morphometric characterization of subglacial bedforms in Scandinavian meltwater corridors

2.1 Study areas

The study areas are located on the crystalline Fennoscandian Shield (*Koistinen et al., 2001*) covered by a layer of subglacial sediments less than 10 m thick and deposited during the Late Weichselian glaciation. The SIS covered Scandinavia entirely and extended to northern continental Europe during the Last Glacial Maximum (LGM) (22 ka BP; *Hughes et al., 2015; Stroeven et al., 2016* for ages), before progressively retreating over Scandinavia between 17 and 9 ka BP (**Fig. 2a**). Within the central part of the SIS, both in Sweden and Finland, hummock tracts and murtoo fields occur in places characterized by rapid SIS retreat corresponding to warmer periods during which the meltwater flow increased ('Bølling-Allerød interstadial', 14.7-13 ka BP and 'early Holocene warming', 11.7-9 ka BP) (*Peterson and Johnson, 2018; Ojala et al., 2019*).

The selected study areas are located along hummock tracts, interpreted as meltwater corridors, where murtoo fields are locally associated with ribbed bedforms (**Fig. 2**). In Sweden, the study areas are located in the southern Swedish highland, south of the Middle Swedish end moraines (12.7 ka BP) related to the southern lobate termination of the SIS (**Fig. 2b; Lundqvist and Wohlfarth, 2000**). The study area in Finland lies in the trunk of the Finnish Lake District Ice Lobe, northwest of the Salpausselkä end moraine zone (12.7 ka BP) and the Central Finland Ice Marginal Formation (11ka BP; *Punkari, 1980*).

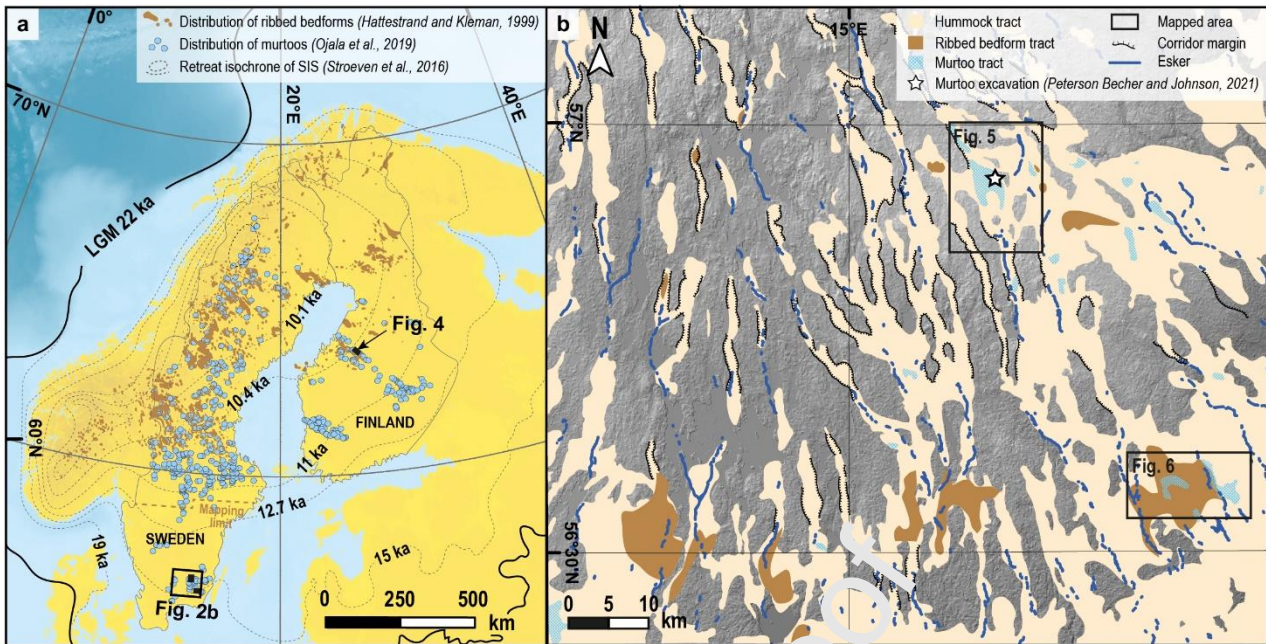


Figure 2. (a) Overview map of northern Europe with selected retreat isochrones of the Scandinavian Ice Sheet (Stroeven *et al.*, 2016), distributions of murtoos (Ojala *et al.*, 2019) and ribbed bedform fields (Hattestrand and Kleman, 1999) in Scandinavia. Black boxes indicate locations of mapped areas. (b) Hillshaded DEM and glacial geomorphological map of the South Swedish uplands illustrating the spatial relationships between eskers, hummock tracts, ribbed bedform tracts and murtoos (modified after Peterson *et al.*, 2017). The white star indicates the location of a murtoo excavated by Peterson Becher and Johnson (2021).

2.2 Method

2.2.1 Data sources and processing

We conducted high-resolution (1: 5 000 to 1: 10 000) mapping from open-data LiDAR-based DEMs available on the online databases of the Geological Survey of Finland (<http://gtkdata.gtk.fi/maankamara/>) and the Swedish Mapping, Cadastral and Land Registration Authority (<https://www.lantmateriet.se/sv/>). From these 2-m LiDAR DEMs, we derived hillshade maps and residual relief maps (Hiller and Smith, 2008) with Geographic Information System (GIS) software.

2.2.2 Bedform delineation and morphometric analysis

Break values of hillshade and residual relief data were delineated manually to produce bedform contours, for which perimeters (P) and areas (A) were measured (Fig. 3a). Lengths of transverse (i.e. transverse to the local ice flow direction), and longitudinal (i.e. parallel to the local ice flow direction) axes were measured using minimum bounding rectangles. Local ice flow directions were determined using streamlined bedforms observed within or in the vicinity of the mapped area. We also drew bedform crest lines by delineating lines of maximum elevation within each contour. Curvilinear and straight lengths of bedform crest lines were measured, using minimum bounding rectangles. The slopes of downstream and upstream edges of bedforms, the wavelength between bedform crest lines and the tip angle of sub-triangular and triangular bedforms were also measured.

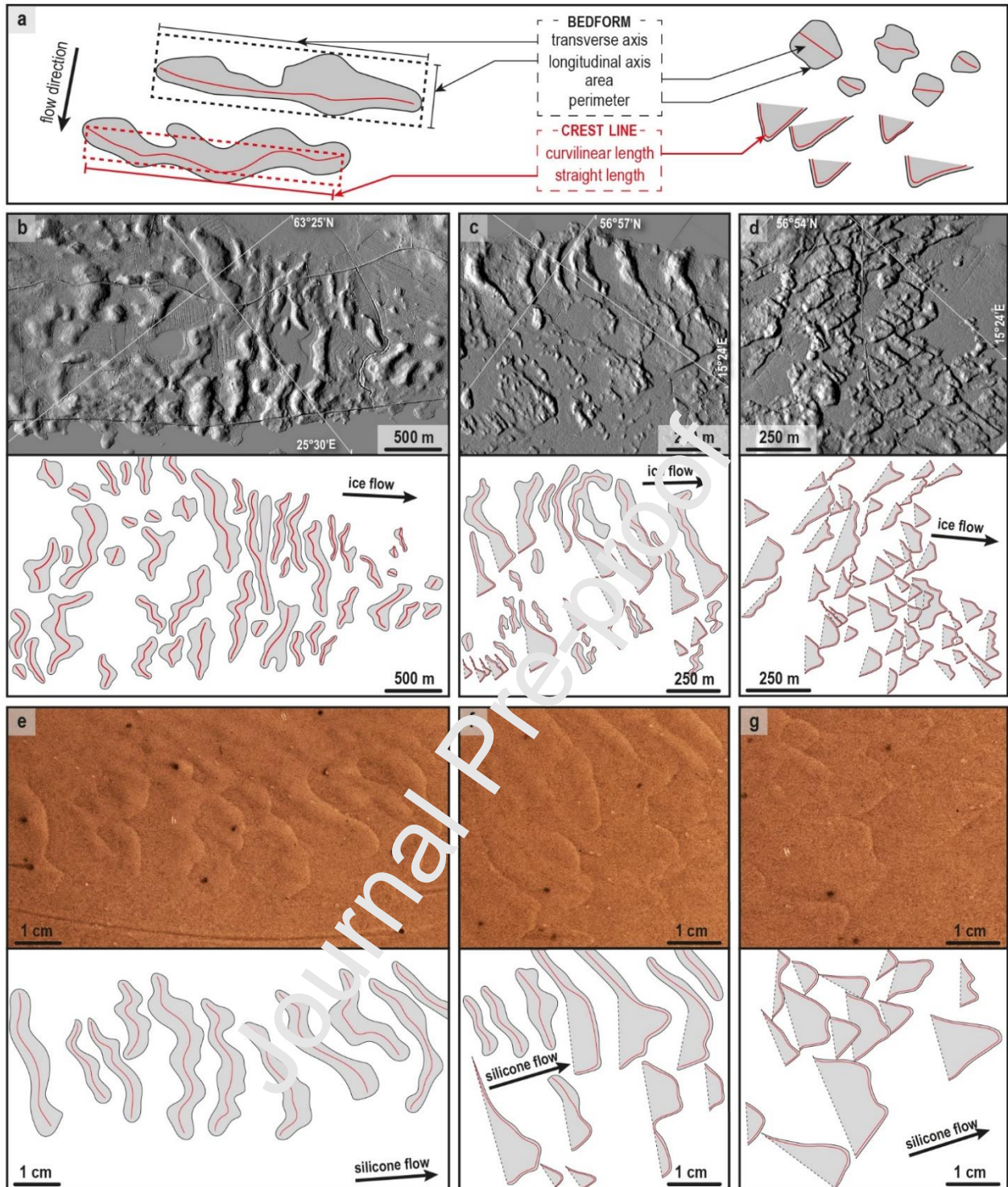


Figure 3. Typical examples of natural (from Finland and Sweden) and experimental bedforms (see Section 3 for experimental description), and our mapping of their morphology as grey polygons with red crest lines. Note the differences in scale. (a) Measurement method of dimensioned morphometric parameters on bedforms and crest lines, which are used for the calculation of the dimensionless indices: elongation, circularity index and sinuosity index. (b) and (e) Natural and experimental ribbed bedforms. (c) and (f) Examples of bedforms spatially-associated with ribbed bedforms and murtoos that display intermediate morphological properties between those of ribbed bedforms and murtoos. These bedforms are named intermediate bedforms. (d) and (g) Fields of natural and experimental murtoos and intermediate bedforms.

From these measurements, we computed three dimensionless morphometric indices that describe bedform differences in shape independently of their differences in size: elongation (equation 1), circularity index (equation 2, modified from *Burgess, 2003*) and sinuosity index (equation 3). Theoretical elongation values range from 0 (for contours strongly elongated parallel to ice flow) to $+\infty$ (for contours strongly elongated orthogonal to ice flow), and a value of 1

corresponds to an isotropic contour. Theoretical circularity index values range from 0 (for strongly non-circular contours) to 1 (for perfectly circular contours). Theoretical sinuosity index values range from 0 (for perfectly straight crestlines) to $+\infty$ (for strongly sinuous crestlines), and a value of 1 corresponds to an equilateral triangular crestline.

$$\text{Elongation (El)} = \text{Transverse axis} / \text{Longitudinal axis} \quad (1)$$

$$\text{Circularity index (I}_{\text{circ}}) = (4\pi A)/P^2 \quad (2)$$

$$\text{Sinuosity index (I}_{\text{sin}}) = ((\text{Curvilinear length}/\text{Straight length}) - 1)/(\sqrt{5} - 1) \quad (3)$$

2.3 Results: Subglacial bedforms along Scandinavian meltwater corridors

2.3.1 Bedform morphometry: a morphometric continuum between ribbed bedforms and murtoos

In the selected study areas, the total number of bedforms identified is 208 (**Figs. 4-6**). Their morphological characteristics are remarkably similar within and between each area, and were therefore compiled in a single database (**Figs. 7-8**). There are no gaps or jumps in the distribution of their morphometric characteristics (**Fig. 8**): all analyzed bedforms stand along a morphometric continuum between three end members, which we schematically portray in the left-hand column of **Fig. 7** and in **Fig. 8**. The 1st end member corresponds to sub-circular bedforms without any preferential orientation showing a circularity index of 1, a sinuosity index close to 0 and an elongation ratio of 1. The 2nd end member corresponds to slightly undulating to linear bedforms transverse to the local ice flow direction with a circularity index close to 0.2, a sinuosity index close to 1 and an elongation ratio of up to 10. The 3rd end member is composed of bedforms displaying an equilateral triangular shape with a circularity index close to 0.8, a sinuosity index of 1 and an elongation ratio of 1.

Between the 1st and 2nd end members lies a category corresponding to regularly-spaced bedforms ($\lambda = \sim 200\text{--}300$ m), mostly transverse to the ice flow direction, with an undulating to linear crest line: we refer to these as ribbed bedforms since they have all the characteristics described by *Dunlop and Clark (2006)* (**Fig. 3b**). Their longitudinal profile is almost symmetrical; in most cases the downstream edge (median slope value = 8.3°) is slightly steeper than the upstream edge (median slope value = 6.5°). Ribbed bedforms are typically 10 m high, 110–275 m long, and 50–110 m wide. Close to the 1st end member, ribbed bedforms are slightly elongated ($El < 2$), non-sinuuous ($I_{\text{sin}} < 0.05$) and highly circular ($I_{\text{circ}} > 0.6$); while they are more elongated ($El > 2$), slightly more sinuous ($0.05 < I_{\text{sin}} < 0.15$) and less circular ($I_{\text{circ}} < 0.6$) close to the 2nd end member. Some ribbed bedforms have experienced morphological transformations that result from their disaggregation (**Fig. 6d**) or breaching (**Fig. 4c**), sometimes splitting initial ribbed bedforms in two parts or more.

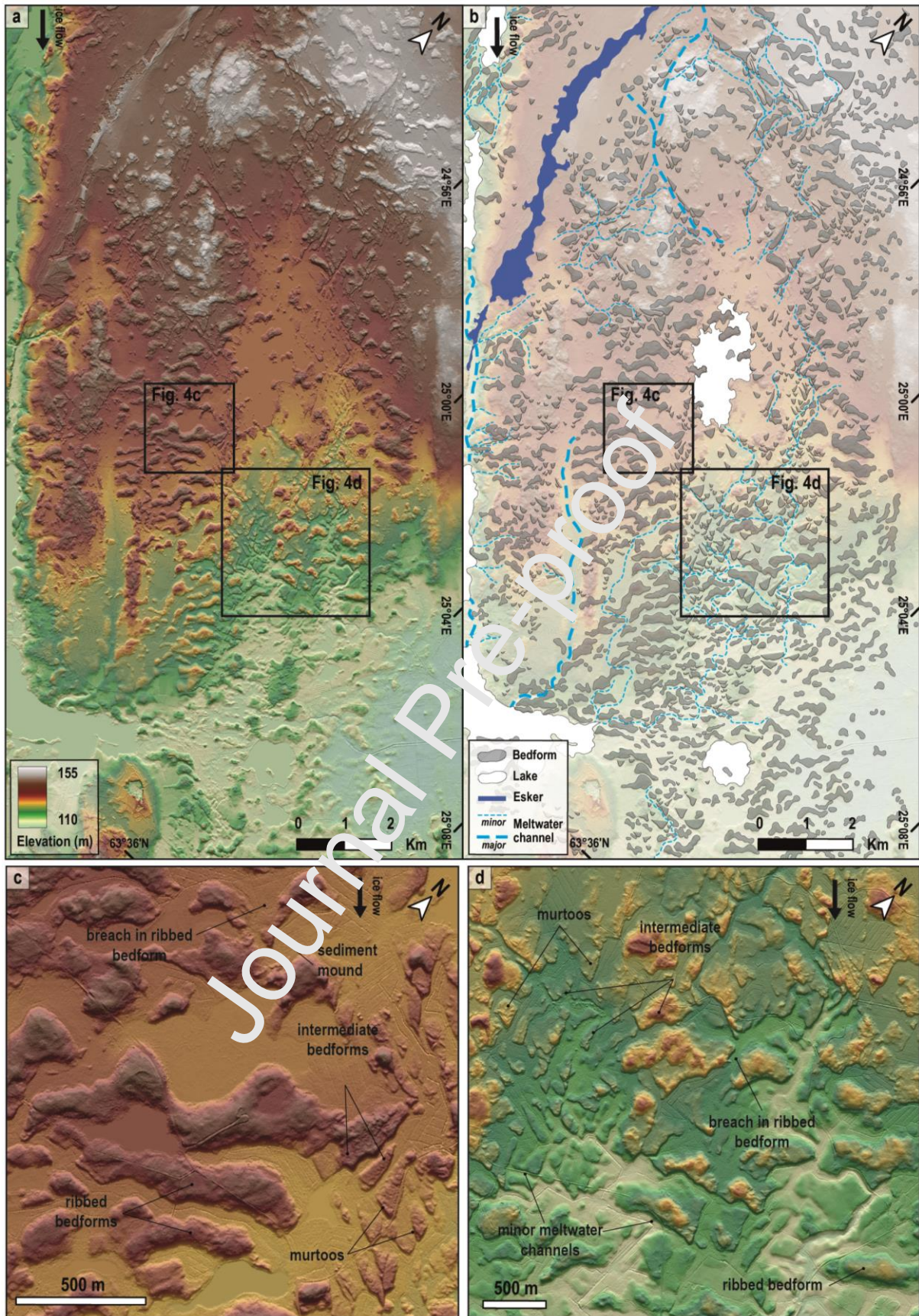


Figure 4. (a) LiDAR DEM and (b) interpretative morphological map with digitized bedforms of a portion of the Finnish Lake District Ice Lobe. (c) and (d) Murtoos occur in close spatial association with ribbed bedforms. Some ribbed bedforms located close to murtoo fields are breached forming sediment mounds in front of their downstream edges. Other bedforms – which we named intermediate bedforms – are spatially associated with ribbed bedforms and murtoos, and characterized by intermediate morphological properties to these two types of bedform. (d) Murtoos and intermediate bedforms are gathered into corridors, often at slightly lower elevations compared with surrounding terrain of ribbed bedforms, and sometimes form a chevron-like geometrical pattern associated with minor meltwater channels.

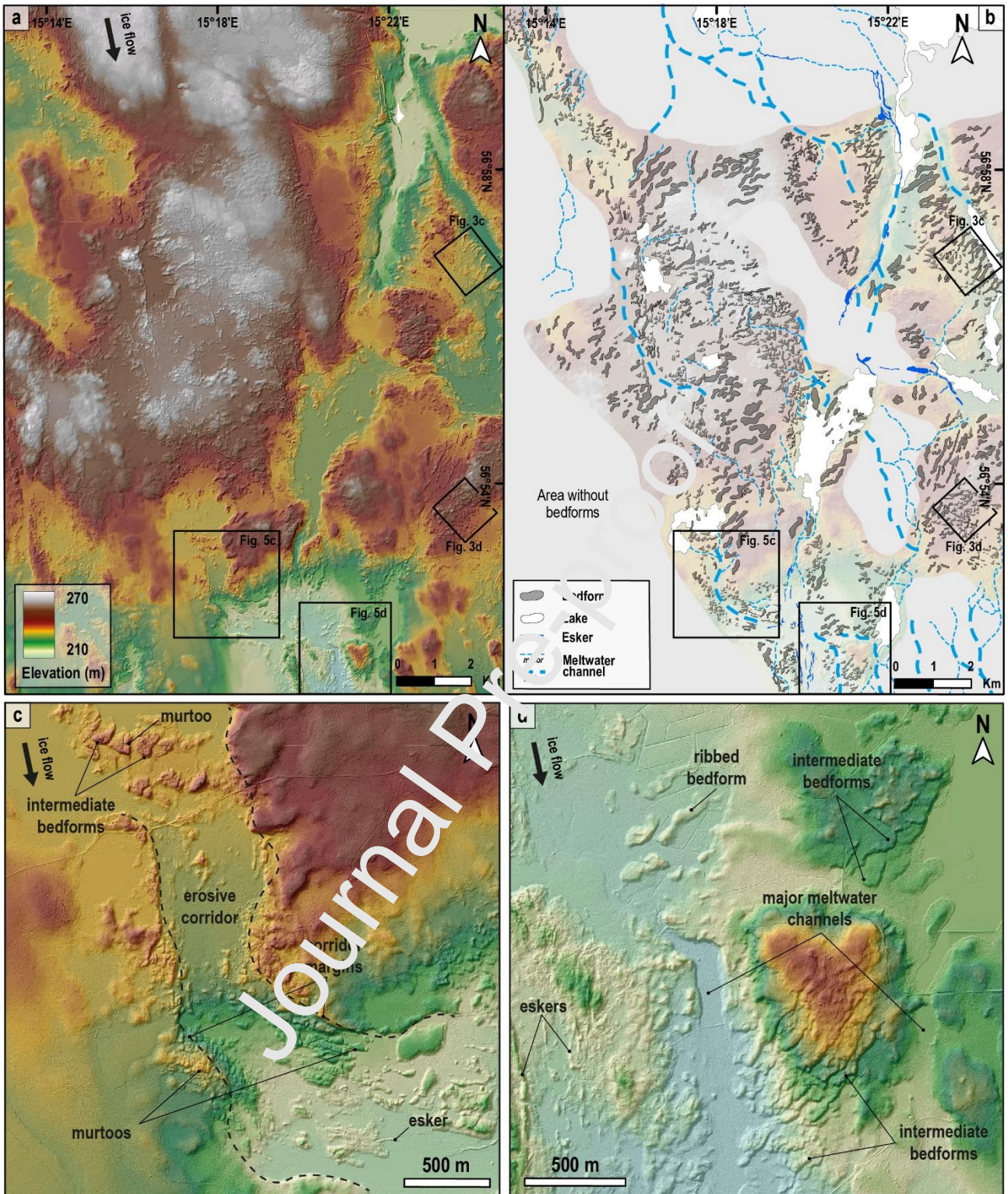


Figure 5. (a) LiDAR DEM and (b) interpretative morphological map with digitized bedforms of a northern portion of the south Sweden Ice Lobe. (c) and (d) Murtoos frequently occur within erosive corridors delimited by sharp margins. In the same field, murtoos are associated with a variety of intermediate bedforms. Major meltwater channels and eskers commonly have a central position in the corridors and are surrounded by ribbed bedforms, murtoos and intermediate bedforms.

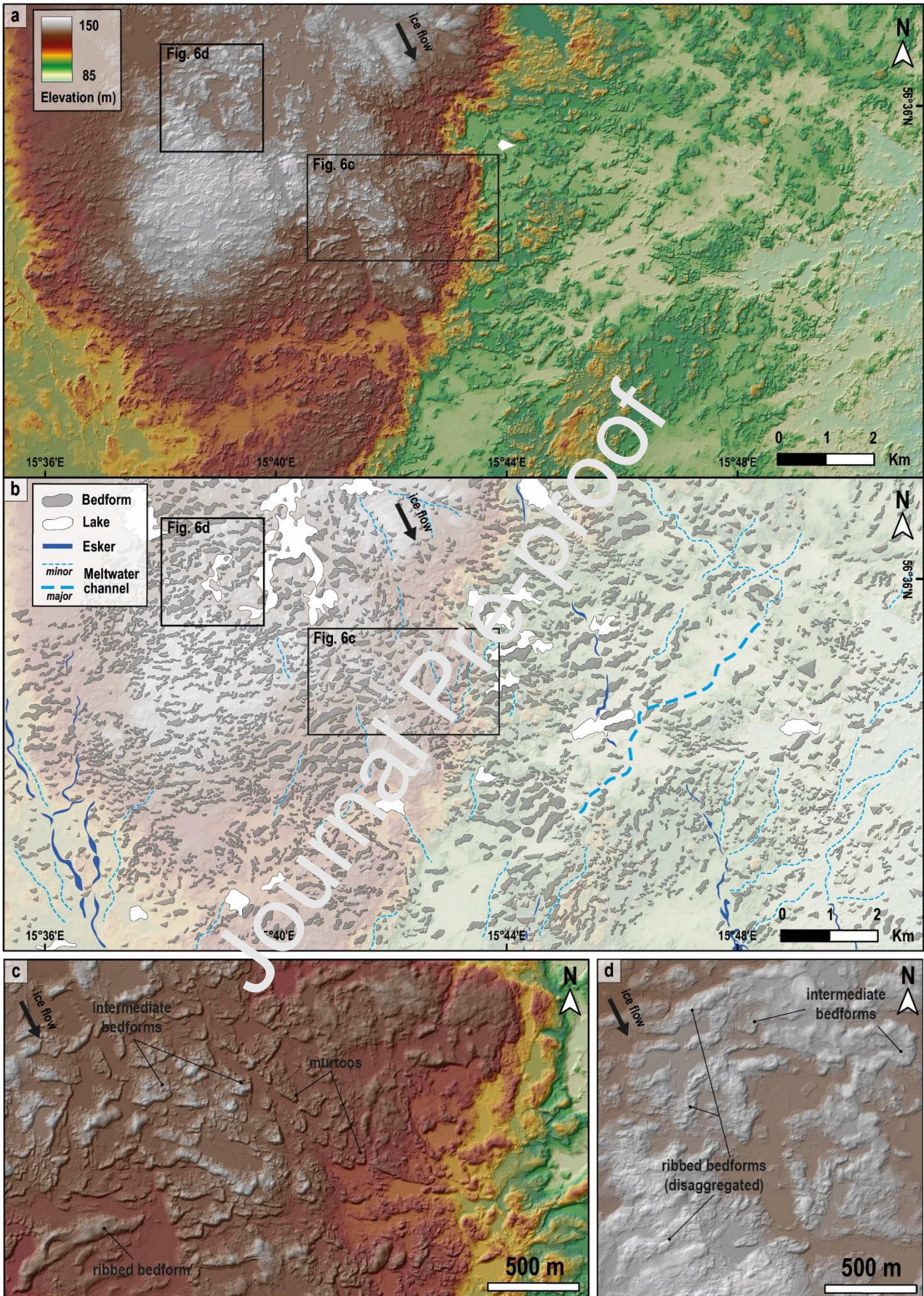


Figure 6. (a) LiDAR DEM and (b) interpretative morphological map with digitized bedforms of a southern portion of the south Sweden Ice Lobe. (c) Murtoos, intermediate bedforms and ribbed bedforms form a morphological transition from the center toward the lateral margin of the murtoo field. (d) Some ribbed bedforms display a disaggregated appearance and are spatially associated with murtoos and intermediate bedforms.

Between the 2nd and 3rd end members, bedforms present morphometric characteristics intermediate between ribbed bedforms and triangular-shaped bedforms and are therefore referred to as intermediate bedforms (**Figs. 3c, 7c, 8b**). Some intermediate bedforms are morphometrically close to ribbed bedforms: they have one or several parts that display a symmetric longitudinal profile and an arcuate crest line transverse to the ice flow direction (i.e. ribbed bedforms), while other parts, cross-cutting or overlapping the latter, show a lobate to triangular form pointing in the downstream direction with an asymmetric longitudinal profile (**Figs. 4c, 5d**). Other bedforms show an overall lobate to irregular triangular shape with a tip pointing in the downstream direction and an opening angle ranging between 70 and 110°. Close to the 3rd end member, we observe regular triangular forms in plan view that are typically 65–120 m long and 40–80 m wide, representing typical morphological values of murtoos measured by *Ojala et al. (2019, 2021)* (**Fig. 3d**). Like murtoos, the triangle tip generally points in the direction of the local ice flow direction, determined through surrounding lineations, and its angle ranges from 56 to 72°, corresponding to the average angle of an equilateral triangle (**Figs. 4c-d, 6c**). The longitudinal axis is almost the bisector of the tip angle and its topographic profile is asymmetric; the downstream edge (mean value = 12°) is steeper than the upstream edge (mean value = 4°). On average, intermediate bedforms are slightly elongated transverse to the ice flow direction ($1 < El < 1.5$), circular ($0.6 < I_{\text{circ}} < 0.8$) and very sinuous ($I_{\text{sin}} > 0.7$) (**Figs. 7c, 8b**). The 3rd end member corresponds to typical murtoos and the intermediate bedforms between ribbed bedforms and murtoos typically correspond to lobate-type murtoos, murtoo-related ridges and to murtoos cross-cutting ribbed bedforms described by *Ojala et al. (2019, 2021)*.

The elongation, sinuosity index and circularity index of the bedforms mapped in the study areas show the existence of a morphometric continuum between three end members: (1) circular bedforms, (2) linear to undulating transverse bedforms, and (3) triangular bedforms pointing in the ice flow direction. The first branch of the morphometric continuum, between the 1st and 2nd end members, illustrates a continuum of ribbed bedforms from circular to transverse and elongated forms. *Greenwood and Clark (2008)* and *Ely et al. (2016)* integrated circular bedforms – also referred to as hummocky-ribbed bedforms (*Hattestrand, 1997; Dunlop and Clark, 2006; Moller and Dowling, 2015*) – in a unique bedform assemblage intimately associated with ribbed bedforms and demonstrated the existence of a morphometric continuum. *Hattestrand (1997)* and *Moller and Dowling (2015)* have previously emphasized that this morphometric continuum corresponds to a genetic continuum related to the development of ribbed bedforms. Therefore, this branch of the morphometric continuum will not be much further discussed here. The second branch, between the 2nd and 3rd end members, illustrates a previously unknown continuum between ribbed bedforms, murtoos and a variety of morphologically intermediate bedforms.

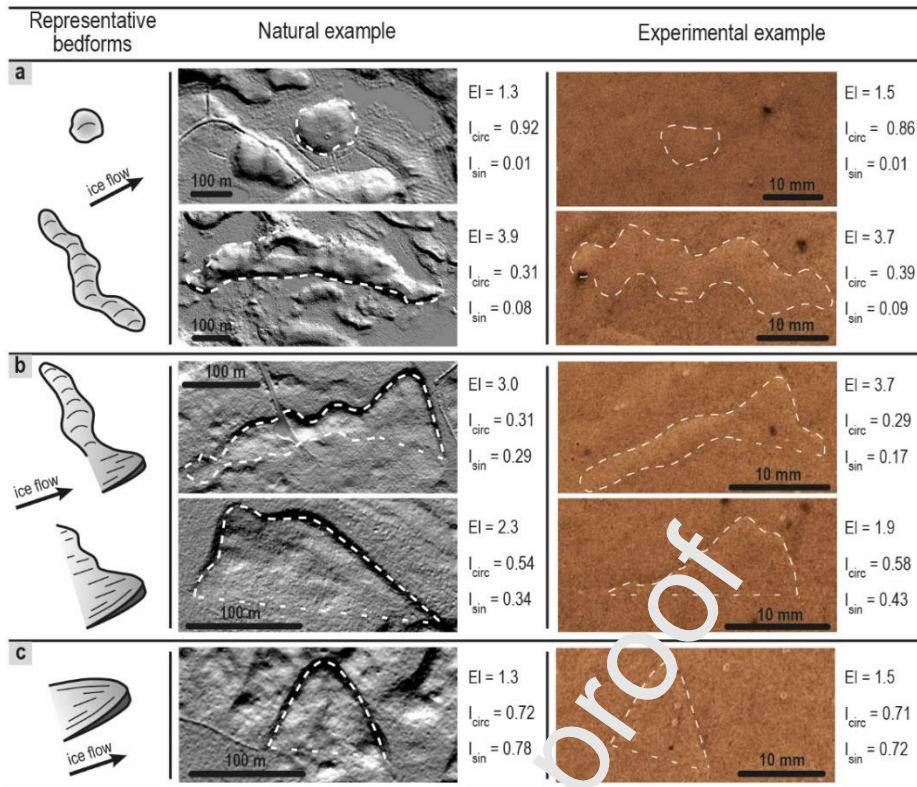


Figure 7. Morphological appearance and morphometric characteristics of typical natural and experimental (a) ribbed bedforms, (b) intermediate bedforms and (c) murtoos.

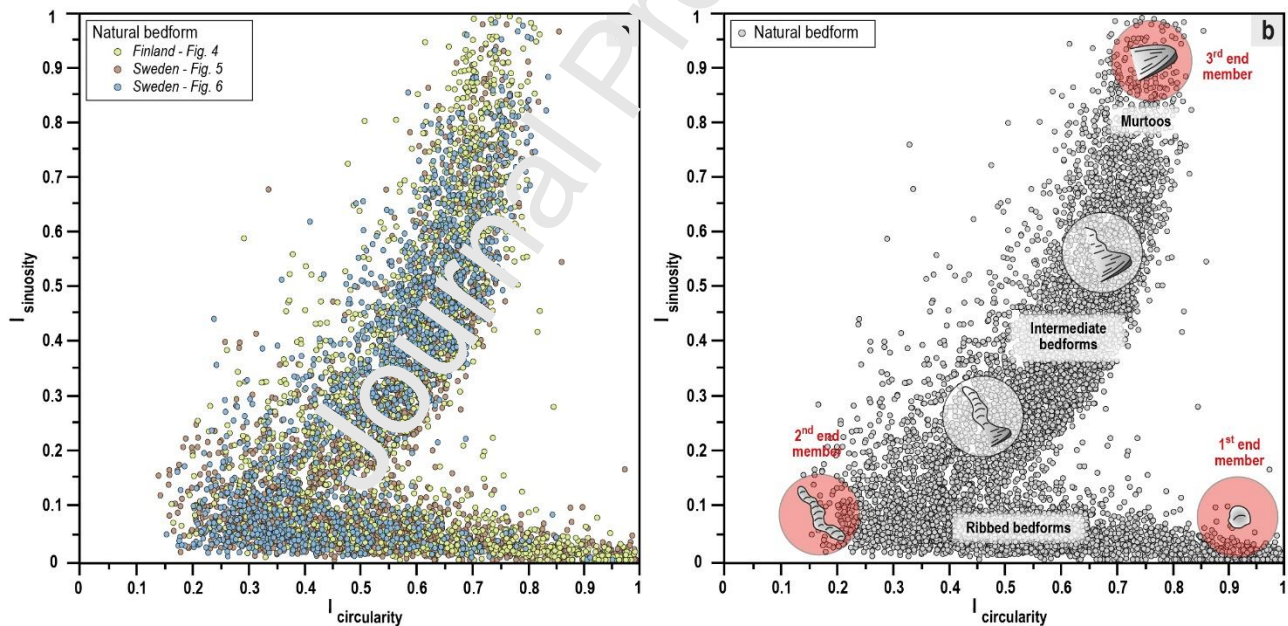


Figure 8. Morphometry of natural bedforms in the Swedish and Finnish study areas. A morphological continuum is observed between three end members (red circles): a continuum of ribbed bedforms with variable circularity (and elongation) and low sinuosity between the 1st and 2nd end members, and a continuum between ribbed bedforms (low circularity and low sinuosity) and murtoos (high circularity and high sinuosity), with a panel of morphologically intermediate bedforms, between the 2nd and 3rd end members.

2.3.2 Spatial distribution of bedforms and their relationship with meltwater corridors

In the mapped areas, where murtoos are observed in spatial association with ribbed bedforms, murtoos and intermediate bedforms gather in fields that are 0.5-2 km wide and 1-4 km long on average and develop parallel to the ice flow direction, preferentially in flat or low-relief areas. Within these fields, bedforms frequently overlap each other

in the downstream direction and exhibit chevron-like patterns (**Fig. 4d**), while others are isolated. Fields of murtoos appear adjacent to or within fields of ribbed bedforms, and in most cases the lateral boundaries between these fields are diffuse and difficult to define (**Figs. 5d, 6c-d**). However, murtoos commonly appear in the core of the fields while the concentration of intermediate bedforms gradually increases toward the field margins (**Fig. 6c**). Boundaries between murtoo fields and ribbed bedform fields are typically defined by bedforms related to breaching, disaggregation, transformation of ribbed bedforms forming an array of intermediate bedforms (**Figs. 4c-d, 6d**).

Edges of murtoos and intermediate bedforms are often delineated by minor meltwater channels – up to 50 m wide and several hundreds of meters long – forming braided systems (**Fig. 4d**) that connect with major meltwater channels few hundreds of meters wide and several kilometers long (**Fig. 5d**). These major meltwater channels frequently cross murtoo fields and are generally orientated parallel to the field margins and to the local ice flow direction. In some places, murtoo fields are delimited by sharp margins related to large erosional meltwater corridors (**Fig. 5c**). Other drainage features are depositional and correspond to eskers in association with murtoos (**Fig. 5d**). Eskers frequently connect with meltwater channels (**Figs. 5b, 6b**) and intersect or overlap murtoos and intermediate bedforms (**Fig. 5c**). These observations show that fields of murtoos and intermediate bedforms are intimately associated with both erosional and depositional drainage features at different scales, while these drainage features are not apparent along adjacent fields of ribbed bedforms.

3 Experimental modeling of subglacial bedforms development along meltwater corridors

We explored experimentally the hypotheses (i) that the spatial relationships described in Section 2.3.2 reflect that murtoo formation involves flooding events along meltwater corridors as suggested by *Mäkinen et al. (2017)*, *Ojala et al. (2019)* and *Peterson Becher and Johnson (2021)*, and (ii) that the morphometric continuum between ribbed bedforms and murtoos described in Section 2.3.1 reflects a genetic continuum. For that purpose, we used an experimental model able to simulate flooding events (*Lelandais et al. 2018*) and ribbed bedform development (*Vérité et al., 2021*)

3.1 Methods: Analog modelling

The experimental model consists of a square box, 2x2 m wide and 5 cm high. The box is filled with a 5 cm thick sand layer (median grain size $d_{med} = 100 \mu\text{m}$) that simulates a flat, deformable, erodible, porous and permeable subglacial bed (**Fig. 9a**) (*Evans et al., 2006*). The bed is saturated and compacted to ensure homogeneous values for its density ($\rho_{bulk} = 2000 \text{ kg}\cdot\text{m}^{-3}$), porosity ($\phi_S = 41 \%$) and permeability ($K_S = 10^{-4} \text{ m}\cdot\text{s}^{-1}$). The ice cap is modelled with a circular layer of viscous and transparent silicone putty (density $\rho_{sil} = 967 \text{ kg}\cdot\text{m}^{-3}$, viscosity $\eta_{sil} = 5.10^4 \text{ Pa}\cdot\text{s}^{-1}$) covering the bed (**Fig. 9b**). Ultraviolet (UV) markers, 1 mm in diameter, are placed with an initial spacing of 5 cm on the surface

of the silicon surface. The subglacial hydrological system is simulated by the injection of a solution of water and UV ink (bulk density $\rho_w = 998 \text{ kg m}^{-3}$) through an injector located below the center of the silicone cap. The injector is 8 mm in diameter and placed at a depth of 1.5 cm below the bed surface. The water injection is regulated by a flowmeter (discharge $Q = 0\text{-}100 \text{ ml min}^{-1}$) and is calculated to allow water flow within the bed and at the silicone-bed interface when water pressure exceeds the combined weight of the bed and silicone layers. Isolated values of the pore water pressure are measured with twelve pressure sensors placed at a depth of 1.5 cm below the bed surface and distributed concentrically at 15 and 30 cm from the central injector (**Fig. 9c**). The photographic set-up and the lighting device, which is composed of white light and UV LEDs that alternate every 15 s, enable simultaneous monitoring of landform development, water distribution and silicone cap dynamics. In UV light, the water distribution along the silicone-bed interface is interpreted through the fluorescence of the injected solution and the positions of UV markers are tracked with a time step of 90 s in order to build interpolated maps of the horizontal velocity (V_{surf}) of the silicone cap surface (**Fig. 9d**). In white light, the transparency of the injected solution and the silicone enables manual mapping of bedform contours and crest lines with a horizontal precision of $\pm 0.1 \text{ mm}$ (**Figs. 3e-g, 9c**). The morphological analysis described in Section 2.2.2 for natural bedforms is applied to experimental bedforms presented in the following section.

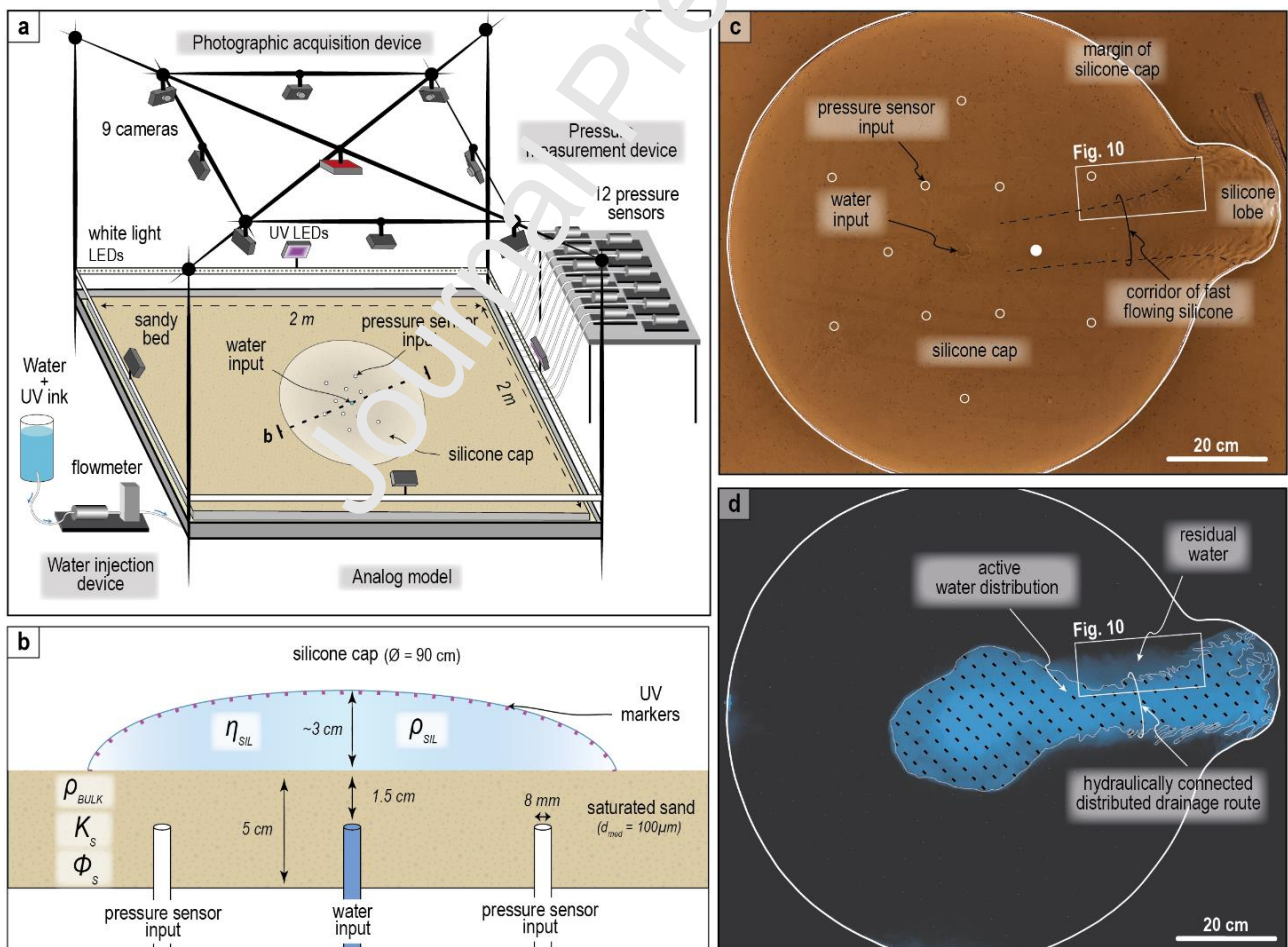


Figure 9. (a) Experimental model, monitoring apparatus and (b) cross-section of the experimental model with the main physical parameters involved (modified after *Vérité et al., 2021*). The flow of a transparent and viscous cap of silicone putty over a deformable and erodible bed made of water-saturated sand is triggered by the injection of a solution of water and UV ink through an injector located in the bed below the center of the silicone cap. The monitoring apparatus is composed of a

lighting set-up, a photographic acquisition device and a pressure measurement device. Surface view of the analog model in (c) white light and (d) UV light. Filled white circle indicates position of pressure sensor input used to produce the plot of pore water pressure in Figure 10. (d) Distribution of water along the silicone-bed interface (stippled area) revealed by the fluorescence of the solution of water and UV ink. Variations in fluorescence intensity indicate if water flow is active or not (i.e. residual water).

The model is designed to simulate the basic physical interactions between an ice cap, a subglacial hydrological system and a sedimentary bed. The bed is composed of wet sand that enables internal deformation by localized and diffuse intergranular shearing, bed-load transport and deposition of grains by flow of water and silicone. The scaling of the experimental model is defined so that the dimensionless ratios between (i) the lobe margin velocity and the incision rate of water channels, and (ii) the bedform wavelength and the cap thickness have similar values in the model and in nature. Limitations stem from the experimental conditions (15–20°C and atmospheric pressure) and rheological properties of the silicone putty (Newtonian viscosity independent of temperature, isotropic and impermeable) that differ from those of ice. The wet and water-saturated sedimentary bed does not allow the reproduction of cold-based subglacial conditions. Temperature-dependent and stress-dependent processes – as heat and shear softening, shear heating and brittle deformation – characterizing glacier ice are not reproducible by the silicone cap. Self-production of meltwater by supraglacial melting, the spatial complexity of basal hydrological systems and ablation processes are not reproducible either (further details regarding scaling and limitations of the experimental model are discussed in *Lelandais et al., 2016* and *Vérité et al., 2021*). Although the experimental model is not a complete and perfectly scaled miniaturization of nature, the landforms obtained experimentally are remarkably similar in appearance to their natural counterparts (**Fig. 3**). These findings strongly support the notion of “unreasonable effectiveness” of experimental modeling as articulated by *Paola et al. (2007)*.

In order to explore the formation of murtoos along meltwater corridors experiencing large, episodic influxes of meltwater, we performed experiments with water discharge scenarios producing repeated flooding events (**Supplementary Data 1**). The water injection scenario aims to produce a dynamic hydrological system and can be divided in two main periods. The first period ($t = 0-90$ min) is characterized by continuous water flow ($Q = 25 \text{ ml min}^{-1}$), while the second period ($t = 90-145$ min) is characterized by discontinued water flow with alternating quiescent and re-injection phases producing three flooding events (**Fig. 10**). The water flow is doubled during the first and the second re-injection phases (i.e. flooding events #1 and #2; $Q = 50 \text{ ml min}^{-1}$) compared to the first period, and quadrupled during the third re-injection phase (i.e. flooding event #3; $Q = 100 \text{ ml min}^{-1}$). The experiments were duplicated to check their reproducibility.

3.2 Results: progressive transformation of ribbed bedforms into murtoos during repeated flooding events

As soon as the water injection starts below the silicone cap, which is flowing under its own weight ($V_{\text{surf}} = 0.2 \times 10^{-2} \text{ mm s}^{-1}$), a circular water pocket forms along the silicone-bed interface below the center of the cap. As the water

pocket grows, reaching 25 to 30 cm in width, the pore water pressure increases below the water pocket. When the pore water pressure exceeds ~ 190 Pa, the water pocket migrates toward the margin of the silicone cap – forming a temporary hydraulically connected distributed drainage route (*Lelandais et al., 2018; Lewington et al., 2020*) – and finally drains outside the cap. From $t = 35$ min to $t = 41$ min, eight water pockets successively migrate and drain. Each drainage route produces a temporary corridor of fast-flowing silicone ($V_{\text{surf}} = 12 \times 10^{-2} \text{ mm s}^{-1}$) forming a lobe at its front. After the pulsed drainage phase with repeated drainage events ($t = 42$ min), a persistent hydraulically connected distributed drainage route develops along the silicone-bed interface. Sustained and focused drainage triggers the formation of a persistent corridor of fast-flowing silicone and enhances the growth rate of the lobe. Beneath the lobe, the drainage route locally channelizes resulting in the formation of two drainage channels. The drainage route is widespread below the corridor of fast flowing silicone but some areas remain dewatered in the periphery of the drainage channels and outside the drainage route. Hereafter, we detail in six stages the evolution of basal hydrology, silicone flow velocity and bedform morphometry along one of the dewatered areas located in the northern periphery of the drainage route (**Figs. 9c-d**).

Stage a (Fig. 10a). As a result of water channelization below the lobe, the silicone cap starts to stabilize at low flow velocity above the drainage route ($t = 54$ min; $V_{\text{surf}} = 6 \times 10^{-2} \text{ mm s}^{-1}$). Contemporaneously, north of the drainage route, a field of subsilicone bedforms develop transverse to the silicone flow (number of bedforms, $n = 12$). The bedforms comprise periodic ridges with a regular wavelength (median $\lambda = 0.9$ cm), a linear crest line (median $I_{\text{sin}} = 0.01$) and an ovoid to slightly elongated shape (median $EI = 2.2$; median $I_{\text{circ}} = 0.52$). The shape and the periodic pattern of these subsilicone bedforms are equivalent to those of ribbed bedforms (**Fig. 7a**) experimentally reproduced by *Vérité et al. (2021)*.

Stage b (Fig. 10b). At the very end of the first period, when water flow is still low and continuous ($t = 90$ min; $Q = 25 \text{ ml min}^{-1}$), and as a result of the sustained channelization below the lobe, the flow velocity of the silicone cap is low and stable ($V_{\text{surf}} = 2\text{-}3.5 \times 10^{-2} \text{ mm s}^{-1}$) over the narrowing drainage route. North of the drainage route, where the silicone-bed interface is coupled, newly-formed ($n = 14$) and previously-formed periodic bedforms ($n = 12$) display a slightly arcuate crest line, symmetrical upstream and downstream edge slopes, a regular wavelength (median $\lambda = 0.9$ cm) and an orientation transverse to the silicone flow direction. Just before the start of the flooding events, the bedforms are more elongated (median $EI = 4.4$), less circular (median $I_{\text{circ}} = 0.34$), and slightly more sinuous (median $I_{\text{sin}} = 0.04$) than in *Stage a*, resulting in bedforms similar in appearance to ribbed bedforms (**Figs. 3e, 7a**).

Stage c (Fig. 10c). After a 10 min period with no water injection during which the silicone cap stops flowing ($V_{\text{surf}} = 0.2 \times 10^{-2} \text{ mm s}^{-1}$), a new injection phase starts at $t = 100$ min ($Q = 50 \text{ ml min}^{-1}$). A new water pocket forms along the silicone-bed interface below the center of the cap. The water pocket grows as the pore water pressure increases until it exceeds ~ 190 Pa at $t = 104$ min, at which point it migrates, overflows the pre-existing drainage route – flooding the

majority of existing ribbed bedforms and increasing the flow velocity of the overlying silicone ($V_{\text{surf}} = 14 \times 10^{-2} \text{ mm s}^{-1}$) – and finally drains outside the cap, producing flooding event #1 and lobe growth. Along the overflowing drainage route, erosion and deposition of sand grains by water flow are responsible for the formation of breaches fragmenting bedforms and sand deposition at the downstream foot of flooded or partially flooded ribbed bedforms. Compared with *Stage b*, the bedforms ($n = 36$) become, on average, more sinuous (median $I_{\text{sin}} = 0.15$), more circular (median $I_{\text{circ}} = 0.41$) but less elongate (median $El = 3.7$), preserving, in most cases, bedforms similar in appearance to sinuous ribbed bedforms. Existing ribbed bedforms outside the overflow route do not experience any shape modification.

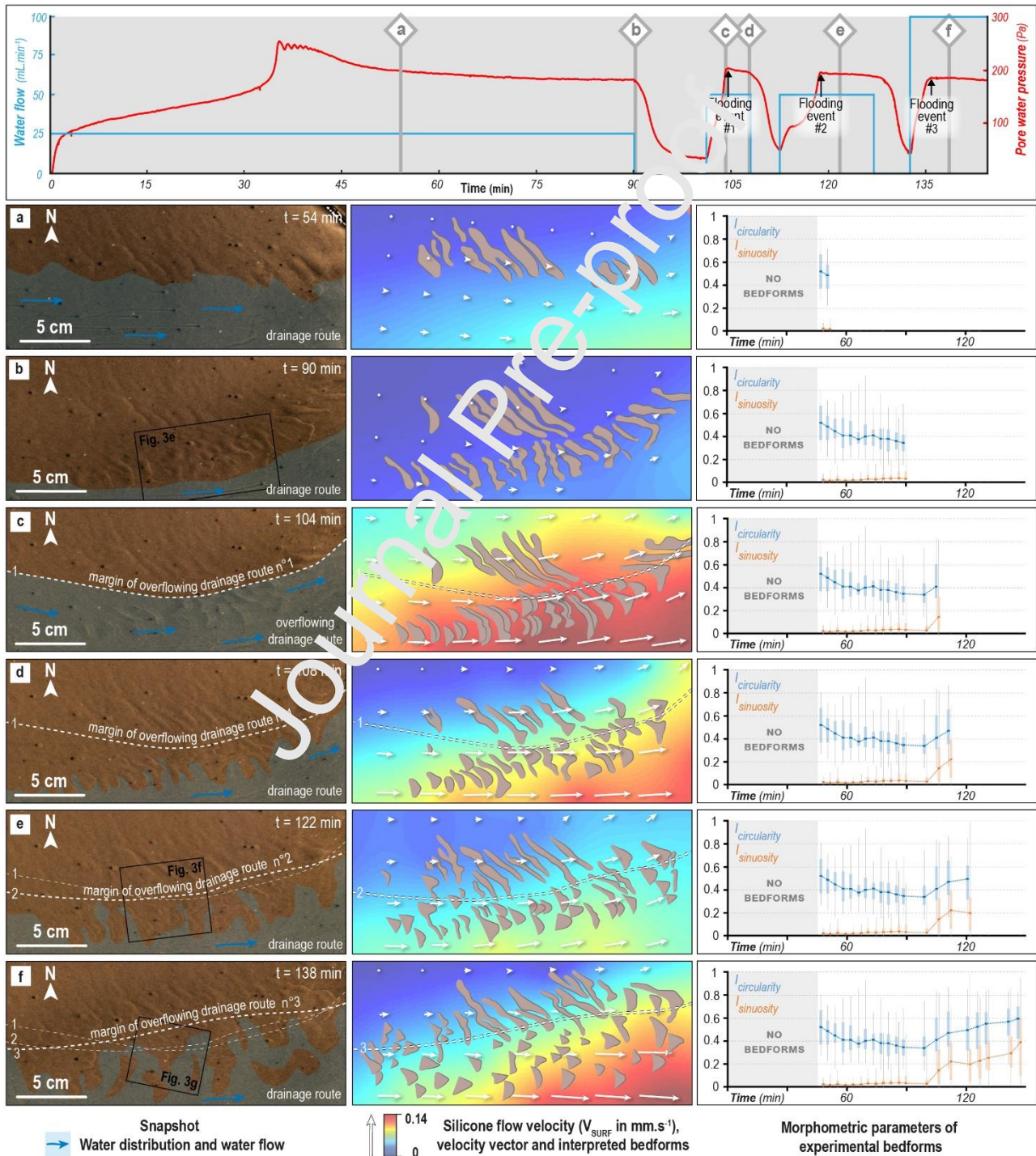


Figure 10. Temporal evolution (*Stages a, b, c, d, e and f*) of the water drainage, the silicone flow dynamics and the bedform morphometry for an experiment comprising steady water input and then repeated flooding events (header graph). Upper

graph shows evolution of water flow injected to the bed (blue line) and pore water pressure (red line) measured below the stream and close to the water injection. Labels (a) to (f) correspond to stages described in section 3.2.

Stages d to f (Figs. 10d-f). After flooding events #1 ($t = 104$ min), #2 ($t = 119$ min) and #3 ($t = 132$ min), which follow a scenario similar to *Stage c*, the drainage route narrows and returns to its initial state: a hydraulically connected distributed drainage route with local areas of silicone-bed coupling. Corridors of fast flowing silicone that developed above the overflowing drainage route during repeated flooding events maintain high velocity ($V_{\text{surf}} = 6-11 \times 10^{-2} \text{ mm}\cdot\text{s}^{-1}$). Along former overflowing drainage routes, where the silicone-bed interface is coupled, crest lines of previously flooded bedforms are stretched in the silicone flow direction and bedforms with an initial ribbed appearance (*Stage b*) record a progressive shape transformation that we describe hereafter.

After flooding event #1 (**Fig. 10d**), one or several parts of some ribbed bedform crest lines are stretched in the silicone flow direction: some parts display lobate crest lines and steep downstream edges, while other parts preserve a ribbed appearance with a linear to arcuate crest line transverse to the flow direction (**Fig. 3f**). Other bedforms and adjacent (formed during flooding events) stretched in the silicone flow direction produced lobate crest lines pointing downstream and steep downstream edges (**Fig. 7b**), similar to lobate-type murtoos described by *Ojala et al. (2021)*. At this stage, experimental bedforms are on average more sinuous (median $I_{\text{sin}} = 0.22$), more circular (median $I_{\text{circ}} = 0.46$) and less elongated (median $El = 3.4$) compared to *Stage c* (**Figs. 10d, 11**). Bedforms located north of the margin of the overflowing drainage route #1 are not reshaped and preserve a ribbed appearance.

After flooding event #2 (**Fig. 10e**), bedforms continue to be partially to entirely stretched in the silicone flow direction, preserving steep downstream edges, inducing a continuous evolution from lobate to sub-triangular crest lines and typically dividing them in two smaller bedforms (**Fig. 7b**). Some minor transverse ridges exhibiting smaller dimensions (1.5 cm long, 0.3 cm wide) than non-flooded ribbed bedforms (5 cm long, 0.6 cm wide) are observed in place of stretched bedforms, suggesting they result from their fragmentation during the flood. After two flooding events, the bedforms are, on average, as sinuous (median $I_{\text{sin}} = 0.21$), more circular (median $I_{\text{circ}} = 0.50$) and less elongate (median $El = 3.1$) than those that experienced just one flood (**Figs. 10e, 11**).

After flooding event #3 (**Fig. 10f**), as a result of the continuous stretching of bedforms along the drainage route, bedforms are almost all characterized by a triangular shape with (i) a tip angle that points downstream and typically lies in between 55 and 75° , and (ii) steep downstream edges, suggesting an asymmetric longitudinal profile. These triangular bedforms sometimes overlap each other, exhibiting a chevron-like pattern (**Figs. 3f**). Their shape and spatial organization resemble those of murtoos described in Scandinavian glacial landsystems (*Ojala et al., 2019*) (**Figs. 3d, 7c**). Some ribbed bedforms with a partial lobate shape still occur along the margin of overflowing drainage route #3 (**Figs. 3f, 7b**). After three flooding events, bedforms are very sinuous (median $I_{\text{sin}} = 0.40$), with higher circularity (median $I_{\text{circ}} = 0.60$) and lower elongation (median $El = 2.5$) values compared with *Stages d* and *e* (**Fig. 11**).

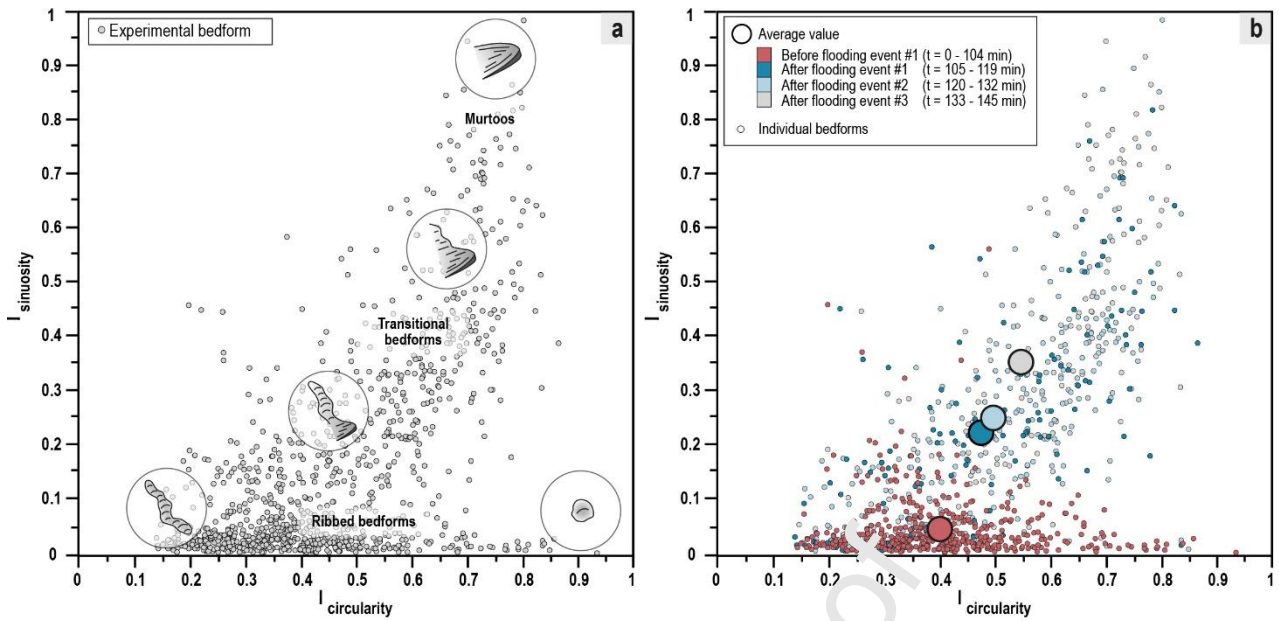


Figure 11. Morphometric plot of experimental bedforms produced and modified under steady water flow input and then during three flooding events of varying durations and magnitudes. A morphometric continuum appears through time and with water input, with no gaps between ribbed bedforms, through transitional bedforms and into murtoos.

To summarize, the repetition of flooding events and intermediate quiescent periods in response to fluctuating water flows triggers an increase in fragmentation and stretching of experimental ribbed bedforms, which successively evolve into transitional forms – such as ribbed bedforms with lobate parts, lobate and sub-triangular bedforms – in a process that finally produces murtoos. This evolution supports the hypothesis that the morphometric continuum described in Section 2.3.1 corresponds to a progressive increase in circularity and sinuosity of ribbed bedforms during successive flooding events (Fig. 11).

4 Discussion

4.1 A continuum between ribbed bedforms and murtoos along meltwater corridors: expression of flooding events

4.1.1 Morphometric comparison of experimental and natural bedforms

Experimental ribbed bedforms display an intermediate elongation (3–5) lying in between natural ribbed bedforms (elongation = 2.9; *Stokes et al., 2016*) and mega-scale transverse bedforms (elongation = 5.7; *Greenwood and Kleman, 2010*). Natural ribbed bedforms mapped in this study display lower elongation (2–3) than their experimental counterparts but correlate with the typical elongation of ribbed moraines mapped by *Dunlop and Clark (2006*; elongation = 2.5). The circularity (0.2–1) and sinuosity (0–0.1) of ribbed bedforms have similar values for natural and experimental forms (Fig. 7a). Morphometric data illustrate that experimental and natural murtoos both display high sinuosity (Fig. 7c; 0.7–1), high circularity (0.65–0.75) and low elongation values (1.3–1.7), which contrast sharply with the range of values characterizing ribbed bedforms (Fig. 7a).

Some transitional experimental bedforms, related to gradual transformation of ribbed bedforms into murtoos, are

morphologically similar to some natural bedforms spatially associated with and morphologically intermediate between ribbed bedforms and murtoos in Scandinavia (**Fig. 7b, 8, 11**). Both natural and experimental bedforms show modified ribbed bedforms with lobate parts, or a lobate to sub-triangular shape (**Figs. 3c, 3f**). They commonly arise on the border of murtoo fields (**Figs. 4c, 10d**) and display sinuosity (0.2–0.7) and circularity (0.3–0.7) values intermediate between those of ribbed bedforms and murtoos (**Fig. 7b**). These bedforms have been either excluded from previous morphological studies since they only share some characteristics with murtoos (*Mäkinen et al., 2017; Ojala et al., 2019*), or for some of them, recently classified as murtoo-related ridges and lobate-type murtoos (*Ojala et al., 2021*). Considering the morphometric similarities between experimental and natural bedforms, these bedforms are therefore both referred to as transitional bedforms with morphological characteristics intermediate between ribbed bedforms and murtoos.

The morphometric comparison of natural and experimental ribbed bedforms, transitional bedforms and murtoos is here limited to three areas located in Finland and Sweden in which all these bedforms coexist. However, even though a correlation in the spatial distribution of ribbed bedforms and murtoos has been observed in several instances (**Fig. 2a; Hättestrand and Kleman, 1999; Ojala et al., 2019**), they do not always coexist along SIS beds (*Peterson et al., 2017; Ahokangas et al., 2021*). Further investigations of paleo-glacial beds, in Scandinavia and North America (i.e. Laurentide Ice Sheet), are necessary to explore the spatial and genetic relationships between these bedforms, notably along meltwater corridors.

4.1.2 Origin of bedform continuum

The spatial association of murtoos with ribbed bedforms (*Peterson et al., 2017; Mäkinen et al., 2017*) and transitional bedforms including, overprinted ribbed bedforms (*Ojala et al., 2019*) and murtoo-related landforms (*Ojala et al., 2021*) has been reported along meltwater corridors in southern SIS areas. While no clear genetic relationships between these different bedforms have been established so far (*Mäkinen et al., 2017; Ojala et al., 2019*), we suggest that they form part of a same morphological and genetic continuum, with some implied commonality of processes. The distribution of values for elongation, sinuosity index and circularity index of both natural and experimental bedforms (**Figs. 8, 11**) indeed reveals a morphometric continuum between ribbed bedforms, transitional bedforms and murtoos. From the evolution of experimental bedforms, we reveal a genetic continuum between ‘ribbed bedform’ and ‘murtoo’ end members, which is materialized by the progressive remobilization of ribbed bedforms into partially remobilized ribbed bedforms (i.e., ribbed bedform with lobate parts), proto murtoos (i.e., lobate to sub-triangular bedform) and murtoos in an environment characterized by transient flooding events (**Fig. 12a**). Based on morphometrics and interpolation of the degree of remobilization (i.e., the magnitude of reshaping) of each experimental bedform at distinct

stages, our experiments suggest that the degree of ribbed bedform remobilization depends on the number of (i) subsilicone floods and (ii) silicone-bed recoupling episodes experienced by any single bedform (**Fig. 13**).

Given the bedform continuum observed in nature is morphometrically identical to that observed in the experiments (**Figs. 8, 11**), we suggest that the processes responsible for the progressive transformation of ribbed bedforms into transitional forms and then into murtoos in the experiments are similar in nature (**Fig. 12b**). Indeed, as demonstrated in *Vérité et al. (2021)*, the processes responsible for the formation of experimental ribbed bedforms are compatible with processes stated to explain the formation of natural ribbed bedforms despite the differences in bedform dimensions, scale of deformation processes and materials (cf. §3.1). In our experiments, some processes such as small-scale channelization and hydrofracturing are not simulated due to insufficient water pressure and homogeneous bed grain size. However, hydrological variations and processes of stretching, erosion and sedimentation are reproduced and responsible for the formation of transitional forms and murtoos, which correlate with processes already described by *Mäkinen et al. (2017)*, *Ojala et al. (2019)* and *Peterson Becher and Johnson (2021)*. Ribbed bedforms are part of this morphometric and genetic continuum only as a starting point representing an initial deformable and erodible sedimentary body later remobilized during flooding and recoupling. Thus, we suggest that the formation of murtoos through the continuous remobilization of ribbed bedforms along Scandinavian meltwater routes depends on the repetition of flooding events. These interpretations have strong implications for deciphering the physical mechanisms operating at the basal interface and the meltwater drainage configurations during the formation of murtoos.

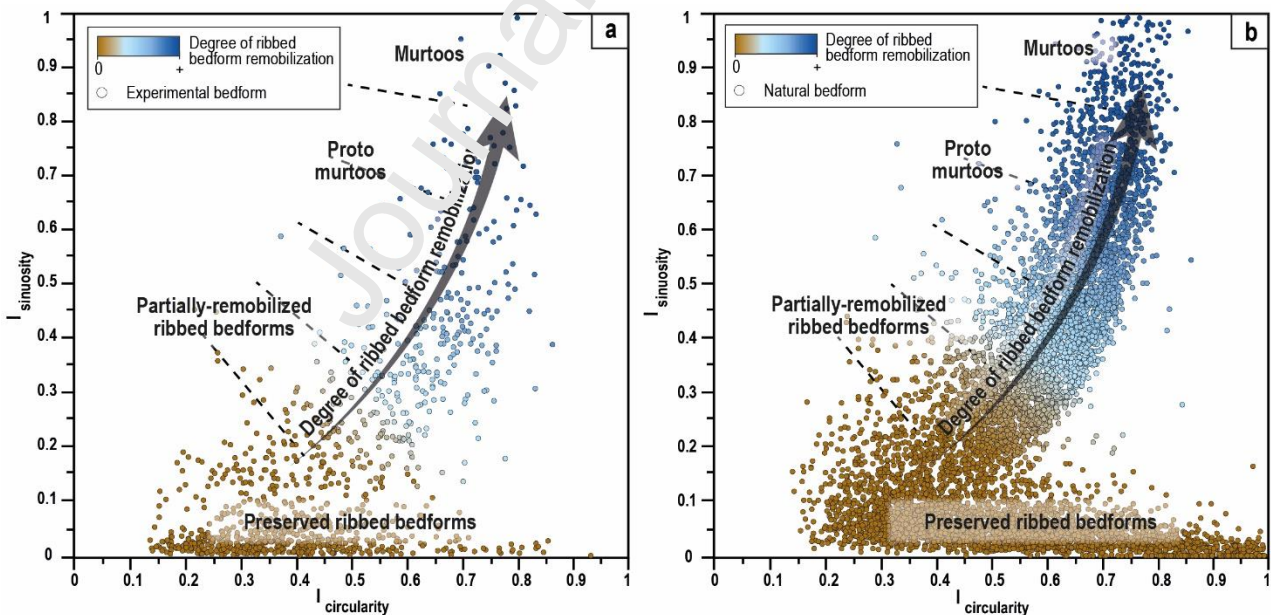


Figure 12. Degree of experimental (a) and natural (b) ribbed bedform remobilization based on the continued increase in circularity and sinuosity indexes from typical ribbed bedforms to typical murtoos during repetitive flooding events.

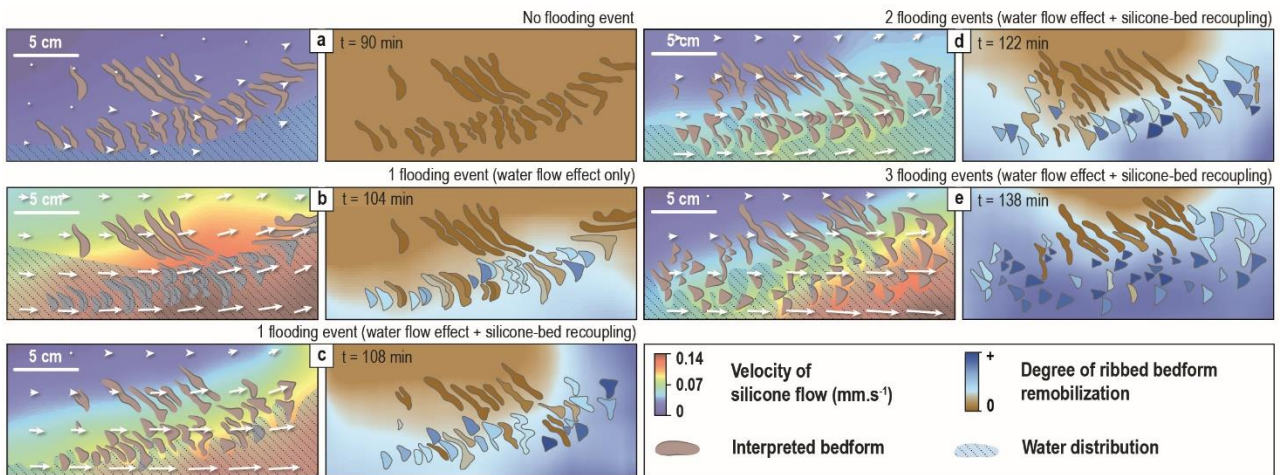


Figure 13. Relationship between the degree of ribbed bedform remobilization (based on the sinuosity and circularity indexes of bedforms; on the right hand side of each panel), the silicone cap dynamics and the subsilicone hydrological system (on the left hand side) for experimental stages presented in Fig. 10.

4.2 A model for the transformation of ribbed bedforms into murtoos along meltwater corridors

Based on the experimental observations, the mapping of Scandinavian ice sheet beds, the bedform continuum depicted in experiments and nature and the current knowledge regarding the sedimentology of murtoos (*Peterson Becher and Johnson, 2021*), we propose a model for the formation of murtoos along meltwater corridors.

Formation of ribbed bedforms (Fig. 14a). A low and constant meltwater discharge at the bed is associated with the development of hydraulically poorly connected distributed drainage routes beneath warm-based ice (*Greenwood et al., 2016*), forming a mosaic of coupling and decoupling zones that can change and migrate through time. Subglacial drainage channels can possibly develop close to the ice sheet margin, where thinner ice inhibits creep closure and hydraulic gradients are steeper. In areas of ice-bed coupling, where the bed undergoes high basal shear stresses, periodic bedforms arise from the deformation of a flat bed (composed of subglacial traction till) sheared by the overlying ice (*Lindén et al., 2008; Fowler and Crampton, 2014; Fannon et al., 2017; Vérité et al., 2021*). Depending on their degree of development, the array of bedforms produced is distributed along a morphological continuum ranging from slightly elongated (i.e. circular) to elongated (i.e. slightly circular) ribbed bedforms (**Fig. 12**). Ribbed bedforms keep growing in dimensions by bed deformation as long as the meltwater flow is low and the ice sheet remains coupled to the crest lines of bedforms (**Figs. 10a-b**). Ribbed bedforms could be a pre-requisite for the initiation of some murtoo fields, and this phase of ribbed bedform formation could occur anytime before the first flooding event.

Erosion and breaching of ribbed bedforms during flooding events (Fig. 14b): Increase in the water discharge delivered to the bed of modern glaciers and ice sheets can occur in response to diurnal, seasonal and long-term thermic fluctuations, and to supraglacial or subglacial lake drainages, producing subglacial floods (*Hubbard et al., 1995; Andrews et al., 2014; Rada and Schoof, 2018; Nanni et al., 2021; Smith et al., 2021*). During subglacial floods (**Fig. 10c**), the preexisting hydraulically poorly connected distributed drainage route overflows and widens the drainage routeway to form a km-wide hydraulically-connected meltwater corridor (*Lewington et al., 2020; Mejia et al., 2021*).

The incapacity of drainage channels to accommodate the sudden increase in water discharge results in widespread ice-bed decoupling, triggering a temporary increase in ice flow velocity and possible surges (*Kamb, 1987; Dunse et al., 2015; Zheng et al., 2019*). Ribbed bedforms are flooded leading to the erosion of their stoss-sides and locally to their sudden breaching (**Fig. 4c**). Erosion, transport and sorting of tills by meltwater are responsible for the re-deposition of sediments on the lee-side toe of ribbed bedforms (**Figs. 4c, 10c**). The erosion of ribbed bedforms is evidenced by their occasional disaggregated appearance, irregularities on their crest lines, their fragmentation related to breaching and their gentler stoss-side slopes (**Fig. 6d**).

Stretching of ribbed bedforms during reorganization of meltwater drainage (Fig. 14c): When the flooding event ceases and as the subglacial drainage reorganizes, the basal meltwater pressure decreases and the ice flow velocity starts to decrease but remains higher than the initial conditions. The km-scale hydraulically well-connected drainage route is envisioned to be characterized by a series of minor meltwater channels (**Fig. 4d**), incising the bed in between bedforms and draining meltwater toward a major and sustained conduit (*Livingston et al., 2020; Mejia et al., 2021*). Within this hydraulically well-connected distributed drainage route the fast-flowing ice recouples to the top of eroded ribbed bedforms and mounds of re-deposited sediments (**Fig. 10d**), transmitting high basal shear stresses to the bed accommodated by soft-bed deformation (*Vérité et al., 2021*). Depending on irregularities along their crest line and the subsequent degree of ice-bed coupling, the ice partially or entirely stretches ribbed bedforms and mounds of re-deposited sediments, forming partially remobilized ribbed bedforms and proto murtoos. The transformation produces more sinuous, more circular and less elongated bedforms, which display steeper edges and develop a lobate tip pointing downstream. Where the ice recouples with the bed, lenses of water-sorted sediments are incorporated into the matrix of subglacial traction till, mainly through soft deformation processes. This correlates with the sedimentological observations in murtoo excavations by *Peterson Becher and Johnson (2021)* that show evidence of deformed silt-sand sediments in a till matrix. As the water pressure builds up in confined water-saturated bed, hydrofracturing develops along lithological interfaces between sorted sediments and subglacial traction till (*Peterson Becher and Johnson, 2021*).

Deposition of traction till during quiescent periods (Fig. 14d): As the water discharge progressively decreases and channelization becomes more efficient along the hydraulically connected distributed drainage route, widespread ice-bed recoupling occurs, thus reducing the ice flow velocity (*Andrews et al., 2014; Mejia et al., 2021; Smith et al., 2021*). The meltwater drainage system, basal conditions and ice flow velocity returns to conditions that prevailed before the flooding event. In response to recoupling, a layer of subglacial traction till sustaining ductile bed deformation can accumulate on top of partially remobilized ribbed bedforms and proto murtoos (*Peterson Becher and Johnson, 2021*). Bedforms along the drainage route undergo little further shape transformation during this stage, probably because basal shear stress transmitted to the bed has decreased in response to a reduction in ice flow velocity.

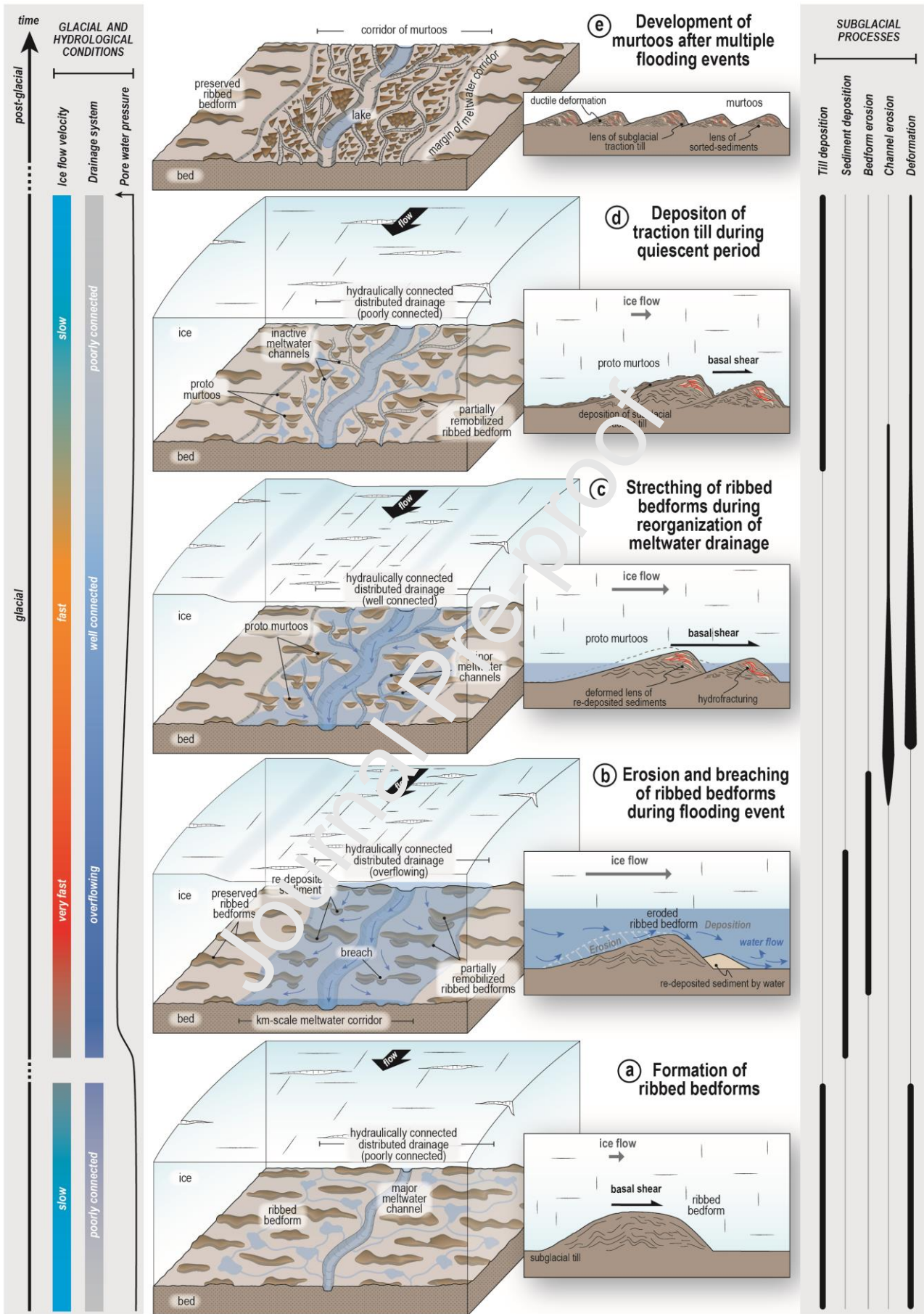


Figure 14. Conceptual model for the formation of murtoos by repeated flooding of ribbed bedforms along subglacial meltwater corridors, based on our natural observations, experimental results, and sedimentological observations from Peterson Becher and Johnson (2021).

Development of murtoos after multiple flooding events (Fig. 14e): The ice sheet demise is associated with the production of large volumes of meltwater that is typically delivered to the bed and transferred subglacially through recurrent episodes of storage and drainage of supra/subglacial lakes (*Greenwood et al., 2016*). Variations in the meltwater discharge and possible flooding can also occur in response to shorter term temperature fluctuations (i.e., diurnal or seasonal) (*Dunse et al., 2015; Smith et al., 2021*). Whatever the frequency of meltwater discharge perturbations, the subglacial bed undergoes multiple alternations between (i) floods characterized by overflow of channels and/or the formation of hydraulically connected distributed drainage routes (**Fig. 14b**) and (ii) quiescent periods characterized by a return to hydraulically poorly connected distributed drainage (**Figs. 14c-d**). Repeated flooding and recoupling result in the progressive fragmentation, reshaping and stretching of ribbed bedforms along meltwater corridors, forming partially remobilized ribbed bedforms, proto murtoos and finally murtoos (**Fig. 12**). Apart from progressive bedform reshaping, *Peterson Becher and Johnson (2021)* demonstrated that repeated flooding and recoupling phases are recorded in the sedimentary core of murtoos where lenses of sorted-sediment are interbedded with layers of subglacial traction till, both ductily deformed and hydrofractured. Through experimental modeling, we confirm conclusions based on geomorphological and sedimentological investigations by *Mäkinen et al. (2017)*, *Peterson et al. (2017)*, *Ojala et al. (2019)* and *Peterson Becher and Johnson (2021)* that murtoos most likely form within a subglacial environment characterized by a transient distributed drainage system focused in meltwater corridors.

Although the presence of ribbed bedforms is a pre-requisite for the formation of murtoos in this model, murtoo fields do not always co-occur with ribbed bedforms along SIS beds (*Peterson et al., 2017; Ahokangas et al., 2021*); this suggests murtoos may not necessarily form from the transformation of ribbed bedforms. Based on morphological characteristics and trench excavations, murtoos have been interpreted to form through alternating deformation of saturated-diamicton and the erosion and deposition of water-sorted sediments (*Mäkinen et al., 2017; Peterson Becher and Johnson, 2021*). These previous interpretations and the frequent absence of ribbed bedforms around murtoo fields might imply that any sedimentary mound, not necessarily a ribbed bedform, could be deformed and stretched to form murtoos. However, it is not known whether murtoos could develop from a flat subglacial bed. Although the proportion of murtoos mapped in association with ribbed bedforms appears to be minor, the multiphase character of the SIS and the tendency to overprint or erase older landforms makes it difficult to determine the true degree of their association. Ribbed bedforms are interpreted to form essentially under low ice flow velocity and basal meltwater flow (*Shaw, 1979; Boulton, 1987; Hattestrand and Kleman, 1999; Lindén et al., 2008; Fowler & Chapwanya, 2014; Vérité et al., 2021*). Murtoo and hummock tracts are interpreted to form during periods of deglaciation when the amount of subglacial meltwater flow increases (*Peterson and Johnson, 2018; Ojala et al., 2019, 2021*). As subglacial bedforms tend to be overprinted over time and ribbed bedforms tend to be remobilized into murtoos, we hypothesize that the "ribbed

bedform" signal could be totally overprinted, thus underestimating the proportion of this murtoo/ribbed bedform spatial relationship.

4.3 Implications for the reconstruction of meltwater corridors

Using combined modelling and palaeo-glacial mapping, we demonstrate that reshaping of ribbed bedforms is linked to repeated changes in subglacial water flow implying that bedforms analysis can be used to better constrain the subglacial hydrological pattern.

Swedish and Finnish murtoos and proto murtoos analyzed in this study gather into elongated corridors (a few kilometer wide and several kilometers long on average) parallel to the ice flow direction within fields of ribbed bedforms. Murtoo fields are also intimately associated with either narrow (up to 50 m wide) or large (few hundreds of meters wide) meltwater channels, supporting a spatial association with meltwater corridors (*Mäkinen et al., 2017; Peterson and Johnson, 2018; Ojala et al., 2021; Ahokangas et al., 2021*). Along meltwater corridors, we also observe that major and minor meltwater channels seem to develop prior and contemporaneously to murtoos while eskers appear to form contemporaneously to or after murtoos (**Figs. 5b, 6**). Based on the transitory hydrological conditions experimentally simulated, the position of murtoo fields relative to SIS end moraine belts confirm they formed along meltwater corridors in relation to long-term perturbations in meltwater discharge during the Bølling-Allerød (14.7 ka) and the early Holocene warmings (11.7 ka) when the margins of the southern Swedish SIS termination and Finnish Lake District Ice Lobe respectively retreated (*Punkari, 1980; Lundqvist, 1986; Hughes et al., 2015; Stroeven et al., 2016*). These inferences imply that murtoos and the transitional forms located along meltwater corridors are attributed to deglaciation, since they are absent along the LGM margin of the SIS, and formed ubiquitously under ice streams, lobes or any front of the ice sheet. This timing relative to the formation of murtoo fields in Scandinavia is in agreement with previous conclusions made by *Ojala et al. (2019)* and *Peterson Becher and Johnson (2021)*. Similarly to *Peterson Becher and Johnson (2021)* and *Ojala et al. (2019)*, we demonstrate that the formation of murtoo fields and meltwater corridors is associated with periodic high meltwater discharge events. This periodicity, possibly related to diurnal, seasonal or long-term thermic fluctuations and the rapid drainage of supraglacially or subglacially stored water, is responsible for the variations in hydraulic connectivity of distributed drainage routes (*Lewington et al., 2020; Ahokangas et al., 2021; Mejia et al., 2021*), resulting in alternating quiescent periods and flooding events. Observations of minor meltwater channels developing along the edges of murtoos and proto murtoos, indicate that the chevron-like pattern of murtoos fields influences the geometry of the drainage system along meltwater corridors, which is neither purely distributed nor purely channelized as mentioned by *Mäkinen et al. (2017)* (**Figs. 4d, 13c**).

The morphological continuum observed along meltwater corridors suggests the progressive remobilization of ribbed bedforms into partially remobilized ribbed bedforms, proto murtoos and murtoos depends on the number (and

probably the magnitude and duration) of flooding events experienced by ribbed bedforms (**Fig. 12**). Even though some murtoo fields strongly correlate with erosive corridors characterized by well-defined margins (**Fig. 5c**), the location of murtoo fields does not seem to be controlled by bed topography (**Figs. 4-6**) implying that drainage routes during successive floods are potentially subject to lateral migration. We suggest that the borders of the hydraulically connected distributed drainage routes vary depending on the migration of the meltwater flood and water discharge (*Rada and Schoof, 2018*).

Journal Pre-proof

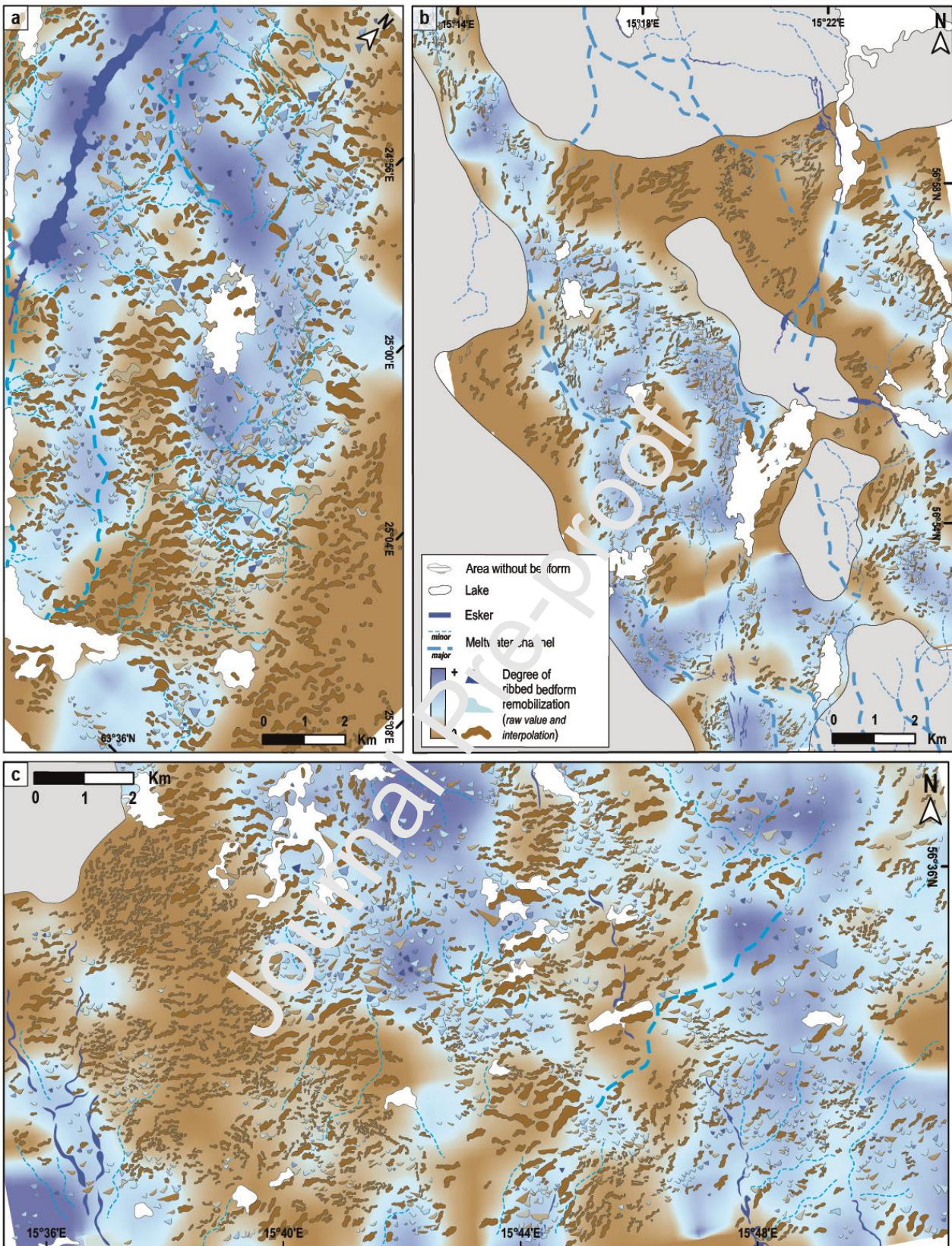


Figure 15. Interpolation maps of the degree of natural ribbed bedform remobilization, based on the sinuosity index and circularity index values of bedforms along Finnish (a) and Swedish zones (b and c).

The number of flooding events that temporarily submerged each bedform along a single meltwater corridor can vary spatially, suggesting that bedforms can experience different stages of morphological evolution according to their positions. Considering the morphometry of experimental bedforms as a proxy for the number of floods recorded along

meltwater corridors (**Figs. 12-13**), interpolation of the degree of remobilization (i.e., degree of reshaping) of each bedform mapped in Scandinavia provides a proxy for (i) the position of meltwater corridors and (ii) the recurrence of floods along a single meltwater corridor (**Fig. 14**). Interpolation maps of the degree of ribbed bedform remobilization also highlight that meltwater corridors are locally slightly more sinuous (from 1.2 to 1.5) compared with the linearity of the ice flow direction (**Fig. 14**), even though they are relatively linear on the scale of an ice sheet (*Peterson et al., 2017*; *Lewington et al., 2020*). Meltwater corridors drawn by the interpolation of the degree of ribbed bedform remobilization are up to 10 km wide, display meandering to anastomosing patterns and longitudinally extend over at least several tens of kilometers across the entire study areas. These meltwater corridors, corresponding to fields of murtoos, proto murtoos and partially remobilized ribbed bedforms, are wider and longer than meltwater corridors reconstructed from murtoo fields only (*Ojala et al. 2019, 2021*; *Ahokangas et al., 2021*), revealing more continuous and more widespread meltwater drainage paths than expected.

5 Conclusion

The combined mapping and modelling approaches in this study enabled the relationship between the evolution of subglacial bedforms and the dynamics of meltwater corridors to be explored. First, we revealed a morphological continuum between ribbed bedforms, transitional forms (i.e. partially remobilized ribbed bedforms and proto murtoos) and murtoos using new dimensionless morphometric parameters (circularity and sinuosity indexes). We demonstrated that bedforms, which have been variously described as ribbed bedforms cross-cut by murtoos (*Ojala et al., 2019*), murtoo-related bedforms and lobate murtoos (*Ojala et al., 2021*), are indeed transitional forms included in a continuous process of murtoo formation from the reshaping of preexisting ribbed bedforms. Second, we interpreted this bedform continuum as the expression of progressive remobilization of ribbed bedforms into murtoos, depending on the recurrence of flooding events that triggers repeated and transitory reorganization of the subglacial hydrological system along meltwater corridors. This dynamic subglacial water system includes alternating phases of (i) significant meltwater discharge, high hydraulic connectivity and ice-bed decoupling (leading to bedform erosion and sediment deposition) and (ii) limited meltwater flow, low hydraulic connectivity and ice-bed recoupling (leading to bedform stretching/deformation). The composite processes (erosion, deposition, deformation) recorded through this morphometric and genetic continuum contribute to better constrain the distribution, evolution and dynamics of meltwater corridors, which are critical for understanding the evolution of past and present day subglacial hydrological configurations and processes over centennial to millennial time-scales and spatially over 100s of km.

Acknowledgment

This study is part of the Ice-Collapse project (The dynamics of ice sheet collapse in deglaciation periods) funded by the French Agence Nationale de la Recherche through grant ANR-18-CE01-0009. This project has benefited from the PALGLAC team of researchers and received funding from the European Research Council (ERC) to Chris Clark under the European Union's Horizon 2020 research and innovation program (grant agreement no. 787263). We thank Mark Johnson and Ivar Benediktsson for their constructive comments that helped to improve the manuscript.

Data availability

All datasets used in this paper are available from the corresponding author on request.

Declaration of competing interests

The authors declare that they have no conflict of interest.

Journal Pre-proof

References

- Ahokangas, E., Ojala, A. E., Tuunainen, A., Valkama, M., Palmu, J. P., Kajuutti, K., & Mäkinen, J. (2021). The distribution of glacial meltwater routes and associated murtoo fields in Finland. *Geomorphology*, 389, 107854.
- Anandakrishnan, S. and Alley, R.B. (1997). Stagnation of ice stream C, West Antarctica by water piracy. *Geophysical Research Letters*, 24(3), pp.265-268.
- Andrews, L. C., Catania, G. A., Hoffman, M. J., Gulley, J. D., Lüthi, M. P., Ryser, C., Hawley, R.L. & Neumann, T. A. (2014). Direct observations of evolving subglacial drainage beneath the Greenland Ice Sheet. *Nature*, 514(7520), 80-83.
- Bell, R. E., Studinger, M., Shuman, C. A., Fahnestock, M. A., & Joughin, I. (2007). Large subglacial lakes in East Antarctica at the onset of fast-flowing ice streams. *Nature*, 445(7130), 904-907.
- Boulton, G. S. (1987). A theory of drumlin formation by subglacial sediment deformation: in Menzies. In J. and Rose, J., eds., *Drumlin Symposium*, Balkema, Rotterdam (pp. 28-80).
- Burgess, D. O., Shaw, J., & Eyton, J. R. (2003). Morphometric comparisons between Rogen terrain and hummocky terrain. *Physical Geography*, 24(4), 319-336.
- Cofaigh, C. Ó. (1996). Tunnel valley genesis. *Progress in physical geography*, 20(1), 1-19.
- Coughlan, M., Tóth, Z., Van Landeghem, K. J., Mccarron, S., & Wheeler, A. J. (2020). Formational history of the Wicklow Trough: a marine-transgressed tunnel valley revealing ice flow velocity and retreat rates for the largest ice stream draining the late-Devensian British–Irish Ice Sheet. *Journal of Quaternary Science*, 35(7), 907-919.
- Dunlop, P., & Clark, C. D. (2006). The morphological characteristics of ribbed moraine. *Quaternary Science Reviews*, 25(13-14), 1668-1691.
- Dunse, T., Schellenberger, T., Hagen, J. O., Kärrholm, A., Schuler, T. V., & Reijmer, C. H. (2015). Glacier-surge mechanisms promoted by a hydro-thermodynamic feedback to summer melt. *The Cryosphere*, 9(1), 197-215.
- Ely, J. C., Clark, C. D., Spagnolo, M., Stokes, C. K., Greenwood, S. L., Hughes, A. L., ... & Hess, D. (2016). Do subglacial bedforms comprise a size and shape continuum?. *Geomorphology*, 257, 108-119.
- Evans, D. J. A., Phillips, E. R., Hiemstra, J. F., & Auton, C. A. (2006). Subglacial till: formation, sedimentary characteristics and classification. *Earth-Science Reviews*, 78(1-2), 115-176.
- Fannon, J. S., Fowler, A. C., & Moyles, J. R. (2017). Numerical simulations of drumlin formation. *Proceedings of the Royal Society A: Mathematical, Physical and Engineering Sciences*, 473(2204), 20170220.
- Fowler, A. C., & Chapwanya, M. (2014). An instability theory for the formation of ribbed moraine, drumlins and mega-scale glacial lineations. *Proceedings of the Royal Society A: Mathematical, Physical and Engineering Sciences*, 470(2171), 20140185.
- Fried, M. J., Carroll, D., Catania, G. A., Sutherland, D. A., Stearns, L. A., Shroyer, E. L., & Nash, J. D. (2019). Distinct frontal ablation processes drive heterogeneous submarine terminus morphology. *Geophysical Research Letters*, 46(21), 12083-12091.
- Greenwood, S. L., & Clark, C. D. (2008). Subglacial bedforms of the Irish ice sheet. *Journal of Maps*, 4(1), 332-357.
- Greenwood, S. L., & Kleman, J. (2010). Glacial landforms of extreme size in the Keewatin sector of the Laurentide Ice Sheet. *Quaternary Science Reviews*, 29(15-16), 1894-1910.
- Greenwood, S.L., Clason, C.C., Helanow, C. and Margold, M. (2016). Theoretical, contemporary observational and palaeo-perspectives on ice sheet hydrology: processes and products. *Earth-Science Reviews*, 155, pp.1-27.
- Hättestrand, C. (1997). Ribbed moraines in Sweden—distribution pattern and palaeoglaciological implications. *Sedimentary Geology*, 111(1-4), 41-56.
- Hättestrand, C., & Kleman, J. (1999). Ribbed moraine formation. *Quaternary Science Reviews*, 18(1), 43-61.

- Hiller, J. K., & Smith, M. (2008). Residual relief separation: digital elevation model enhancement for geomorphological mapping. *Earth Surface Processes and Landforms*, 33(14), 2266-2276.
- Hubbard, B. P., Sharp, M. J., Willis, I. C., Nielsen, M., & Smart, C. C. (1995). Borehole water-level variations and the structure of the subglacial hydrological system of Haut Glacier d'Arolla, Valais, Switzerland. *Journal of Glaciology*, 41(139), 572-583.
- Hughes, O. L. (1964). Surficial geology, Nichicun-Kaniapiskau map area, Quebec. *Geological Survey of Canada Bulletin*, 106, 18pp.
- Hughes, A. L., Gyllencreutz, R., Lohne, Ø. S., Mangerud, J., & Svendsen, J. I. (2016). The last Eurasian ice sheets—a chronological database and time-slice reconstruction, DATED-1. *Boreas*, 45(1), 1-45.
- Iken, A., & Bindschadler, R. A. (1986). Combined measurements of subglacial water pressure and surface velocity of Findelengletscher, Switzerland: conclusions about drainage system and sliding mechanism. *Journal of Glaciology*, 32(110), 101-119.
- Irvine-Fynn, T. D., Hodson, A. J., Moorman, B. J., Vatne, G., & Hubbard, A. L. (2011). Polythermal glacier hydrology: a review. *Reviews of Geophysics*, 49(4).
- Kamb, B. (1987). Glacier surge mechanism based on linked cavity configuration of the basal water conduit system. *Journal of Geophysical Research: Solid Earth*, 92(B9), 9083-9100.
- Kleman, J., & Hättestrand, C. (1999). Frozen-bed Fennoscandian and Laurentide ice sheets during the Last Glacial Maximum. *Nature*, 402(6757), 63-66.
- Koistinen, T., Stephens, M. B., Bogatchev, V., Nordgulen, Ø., Wennerström, M., & Korhonen, J. (2001). Geological map of the Fennoscandian Shield 1: 2 000 000. Espoo: Geological Survey of Finland, Trondheim: Geological Survey of Norway, Uppsala: Geological Survey of Sweden, Moscow: Ministry of Natural Resources of Russia.
- Lelandais, T., Mourgues, R., Ravier, É., Pochat, S., Strzermynski, P., & Bourgeois, O. (2016). Experimental modeling of pressurized subglacial water flow: Implications for tunnel valley formation. *Journal of Geophysical Research: Earth Surface*, 121(11), 2022-2041.
- Lelandais, T., Ravier, É., Pochat, S., Bourgeois, O., Clark, C., Mourgues, R., & Strzermynski, P. (2018). Modelled subglacial floods and tunnel valleys control the life cycle of transitory ice streams. *The Cryosphere*, 12(8), 2759-2772.
- Lewington, E.L., Livingstone, S.J., Sole, A.J., Clark, C.D. and Ng, F.S. (2019). An automated method for mapping geomorphological expressions of former subglacial meltwater pathways (hummock corridors) from high resolution digital elevation data. *Geomorphology*, 339, pp.70-86.
- Lewington, E.L., Livingstone, S.J., Clark, C.D., Sole, A.J. and Storrar, R.D. (2020). A model for interaction between conduits and surrounding hydraulically connected distributed drainage based on geomorphological evidence from Keewatin, Canada. *The Cryosphere*, 14(9), pp.2949-2976.
- Lindén, M., Möller, P., & Adrielsson, L. (2008). Ribbed moraine formed by subglacial folding, thrust stacking and lee-side cavity infill. *Boreas*, 37(1), 102-131.
- Lundqvist, J. (1969). Problems of the so-called Rogen moraine (pp. 1-32). Svensk reproduktions AB (distr.).
- Lundqvist, J. (1986). Late Weichselian glaciation and deglaciation in Scandinavia. *Quaternary Science Reviews*, 5, 269-292.
- Lundqvist, J. (1989). Rogen (ribbed) moraine—identification and possible origin. *Sedimentary Geology*, 62(2-4), 281-292.
- Lundqvist, J., & Wohlfarth, B. (2000). Timing and east–west correlation of south Swedish ice marginal lines during the Late Weichselian. *Quaternary Science Reviews*, 20(10), 1127-1148.

- Mäkinen, J., Kajuutti, K., Palmu, J. P., Ojala, A., & Ahokangas, E. (2017). Triangular-shaped landforms reveal subglacial drainage routes in SW Finland. *Quaternary Science Reviews*, 164, 37-53.
- Mejía, J. Z., Gulley, J. D., Trunz, C., Covington, M. D., Bartholomaeus, T. C., Xie, S., & Dixon, T. (2021). Isolated cavities dominate Greenland Ice Sheet dynamic response to lake drainage. *Geophysical Research Letters*, e2021GL094762.
- Möller, P., & Dowling, T. P. (2015). The importance of thermal boundary transitions on glacial geomorphology; mapping of ribbed/hummocky moraine and streamlined terrain from LiDAR, over Småland, South Sweden. *Gff*, 137(4), 252-283.
- Moon, T., Joughin, I., Smith, B., Van Den Broeke, M. R., Van De Berg, W. J., Noël, B., & Usher, M. (2014). Distinct patterns of seasonal Greenland glacier velocity. *Geophysical research letters*, 41(20), 7209-7216.
- Nanni, U., Gimbert, F., Roux, P., & Lecointre, A. (2021). Observing the subglacial hydrology network and its dynamics with a dense seismic array. *Proceedings of the National Academy of Sciences*, 118(28).
- O'Connor, J. E., Baker, V. R., Waitt, R. B., Smith, L. N., Cannon, C. M., George, D. L., & Denlinger, R. P. (2020). The Missoula and Bonneville floods—A review of ice-age megafloods in the Columbia River basin. *Earth-Science Reviews*, 208, 103181.
- Ojala, A.E., Peterson, G., Mäkinen, J., Johnson, M.D., Kajuutti, K., Palmu, J.P., Ahokangas, E. and Öhrling, C. (2019). Ice-sheet scale distribution and morphometry of triangular-shaped hummocks (murtoos): a subglacial landform produced during rapid retreat of the Scandinavian Ice Sheet. *Annals of Glaciology*, 60(80), pp.115-126.
- Ojala, A. E., Mäkinen, J., Ahokangas, E., Kajuutti, K., Valkonen, M., Tuunainen, A., & Palmu, J. P. (2021). Diversity of murtoos and murtoo-related subglacial landforms in the Finnish area of the Fennoscandian Ice Sheet. *Boreas*.
- Paola, C., Straub, K., Mohrig, D., & Reinhardt, J. (2009). The “unreasonable effectiveness” of stratigraphic and geomorphic experiments. *Earth-Science Reviews*, 97(1-4), 1-43.
- Peterson, G. and Johnson, M.D. (2018). Hummock corridors in the south-central sector of the Fennoscandian ice sheet, morphometry and pattern. *Earth Surface Processes and Landforms*, 43(4), pp.919-929.
- Peterson, G., Johnson, M.D. and Smith, C.A. (2017). Glacial geomorphology of the south Swedish uplands—focus on the spatial distribution of hummock tracts. *Journal of Maps*, 13(2), pp.534-544.
- Peterson Becher, G.P. and Johnson, M.D. (2021). Sedimentology and internal structure of murtoos-V-shaped landforms indicative of a dynamic subglacial hydrological system. *Geomorphology*, 380, p.107644.
- Punkari, M. (1980). The ice lobes of the Scandinavian ice sheet during the deglaciation in Finland. *Boreas*, 9(4), 307-310.
- Rada, C., & Schoof, C. (2018). Channelized, distributed, and disconnected: subglacial drainage under a valley glacier in the Yukon. *The Cryosphere*, 12(8), 2609-2636.
- Rampton, V.N. (2000). Large-scale effects of subglacial meltwater flow in the southern Slave Province, Northwest Territories, Canada. *Canadian Journal of Earth Sciences*, 37(1), pp.81-93.
- Schroeder, D. M., Blankenship, D. D., & Young, D. A. (2013). Evidence for a water system transition beneath Thwaites Glacier, West Antarctica. *Proceedings of the National Academy of Sciences*, 110(30), 12225-12228.
- Sharpe, D. R., Lesemann, J. E., Knight, R. D., & Kjarsgaard, B. A. (2021). Regional stagnation of the western Keewatin ice sheet and the significance of meltwater corridors and eskers, northern Canada. *Canadian Journal of Earth Sciences*, 99(999), 1-22.
- Shaw, J. (1979). Genesis of the Sveg tills and Rogen moraines of central Sweden: a model of basal melt out. *Boreas*, 8(4), 409-426.
- Shaw, J. (2002). The meltwater hypothesis for subglacial bedforms. *Quaternary International*, 90(1), 5-22.

- Simkins, L. M., Anderson, J. B., Greenwood, S. L., Gonnermann, H. M., Prothro, L. O., Halberstadt, A. R. W., ... & DeConto, R. M. (2017). Anatomy of a meltwater drainage system beneath the ancestral East Antarctic ice sheet. *Nature Geoscience*, 10(9), 691-697.
- Slater, D. A., Nienow, P. W., Cowton, T. R., Goldberg, D. N., & Sole, A. J. (2015). Effect of near-terminus subglacial hydrology on tidewater glacier submarine melt rates. *Geophysical Research Letters*, 42(8), 2861-2868.
- Smith, L. C., Andrews, L. C., Pitcher, L. H., Overstreet, B. T., Rennermalm, Å. K., Cooper, M. G., Cooley, S.W., Ryan, J.C., Miège, C., Kershner, C. & Simpson, C. E. (2021). Supraglacial river forcing of subglacial water storage and diurnal ice sheet motion. *Geophysical Research Letters*, 48(7), e2020GL091418.
- Smith-Johnsen, S., Fleurian, B. D., Schlegel, N., Seroussi, H., & Nisancioglu, K. (2020). Exceptionally high heat flux needed to sustain the Northeast Greenland Ice Stream. *The Cryosphere*, 14(3), 841-854.
- St-Onge, D.A. (1984). Surficial deposits of the Redrock Lake area, District of Mackenzie. *Current Research, Part A; Geological Survey of Canada, Paper*, pp.271-276.
- Stokes, C. R., Margold, M., & Creyts, T. T. (2016). Ribbed bedforms on palaeo-ice stream beds resemble regular patterns of basal shear stress ('traction ribs') inferred from modern ice streams. *Journal of Glaciology*, 62(234), 696-713.
- Storrar, R.D. and Livingstone, S.J. (2017). Glacial geomorphology of the northern Kivalliq region, Nunavut, Canada, with an emphasis on meltwater drainage systems. *Journal of Maps*, 1, (2), pp.153-164.
- Stroeven, A.P., Hättestrand, C., Kleman, J., Heyman, J., Fabel, D., Fredin, O., Goodfellow, B.W., Harbor, J.M., Jansen, J.D., Olsen, L. and Caffee, M.W. (2016). Deglaciation of Fennoscandia. *Quaternary Science Reviews*, 147, pp.91-121.
- Utting, D.J., Ward, B.C. and Little, E.C. (2009). Genesis of hummocks in glaciofluvial corridors near the Keewatin Ice Divide, Canada. *Boreas*, 38(3), pp.471-481.
- Vérité, J., Ravier, É., Bourgeois, O., Pochat, S., Lalandais, T., Mourgues, R., Clark, C.D., Bessin, P., Peigné, D. & Atkinson, N. (2021). Formation of ribbed bedforms below shear margins and lobes of palaeo-ice streams. *The Cryosphere*, 15(6), 2889-2916.
- Williams, J. J., Gourmelen, N., & Nienoja, P. (2020). Dynamic response of the Greenland ice sheet to recent cooling. *Scientific reports*, 10(1), 1-11.
- Zheng, W., Pritchard, M. E., Willis, M. J., & Stearns, L. A. (2019). The possible transition from glacial surge to ice stream on Vavilov ice cap. *Geophysical Research Letters*, 46(23), 13892-13902.

Highlights

- High resolution mapping of ribbed bedforms and murtoos in Sweden and Finland
- Modelling reproduces murtoos by erosion/deposition/deformation of ribbed bedforms
- New morphometric parameters show a bedform continuum corresponding to the progressive transformation of ribbed bedforms into murtoos
- This continuum reveals subglacial drainage reorganization during repeated flooding
- We provide key criteria to constrain magnitudes, durations and frequencies of subglacial floods in palaeo-meltwater corridors

Journal Pre-proof